Applied Catalysis B: Environmental 300 (2022) 120744

Contents lists available at ScienceDirect

Applied Catalysis B: Environmental

journal homepage: www.elsevier.com/locate/apcatb

Heterogeneous activation of peroxymonosulfate by natural chalcopyrite for efficient remediation of groundwater polluted by aged landfill leachate

Hongxi Wang [a,b,c], Bing Liao [a,b,c,*], Mengyao Hu [a,b,c], Yulu Ai [a,b,c], Lijia Wen [a,b,c], Shuang Yang [a,b,c], Zhong Ye [a,b,c], Jie Qin [a,b,c], Guo Liu [a,b,c,*]

[a] State Key Laboratory of Geohazard Prevention and Geoenvironment Protection, Chengdu University of Technology, Chengdu 610059, China
[b] State Environmental Protection Key Laboratory of Synergetic Control and Joint Remediation for Soil & Water Pollution, Chengdu University of Technology, Chengdu 610059, China
[c] College of Ecology and Environment, Chengdu University of Technology, Chengdu 610059, China

ARTICLE INFO

Keywords:
Aged landfill leachate
Groundwater
Natural chalcopyrite
Peroxymonosulfate
Advanced oxidation technology

ABSTRACT

Natural chalcopyrite (NCP) was used as a low-cost and efficient activator of peroxymonosulfate (PMS) to repair groundwater polluted by aged landfill leachate. The optimal remediation effect of polluted groundwater was achieved at pH 8, PMS concentration 25 mM and NCP dosage 10 g/L via response surface method. The excellent performance of NCP was mainly Fe^{3+}/Fe^{2+} and Cu^{2+}/Cu^{+} cycles promoted by sulfur species, which was investigated via XPS analysis. Furthermore, the transformation of $SO_4^{\bullet-}$, $^{\bullet}OH$ and $O_2^{\bullet-}$ were clarified by quenching experiments and ESR. The conversion of organics was revealed by UV–vis spectra and three-dimensional fluorescence spectra. Moreover, the toxicity of polluted groundwater after remediation was significantly reduced through the growth of *Chlorella pyrenoidosa*. Finally, the flowing experiment using NCP/sand column showed that NCP could effectively activate PMS and thereby restore polluted groundwater.

1. Introduction

Landfill leachate, as the product of municipal solid waste (MSW) long-term landfills, contains a large number of refractory organic pollutants, inorganic salts and heavy metals, which have strong acute and chronic toxicity to organisms and human body [1,2]. According to different landfill years, landfill leachate can be divided into three categories: young leachate (< 5 years), intermediate leachate (from 5 to 10 years) and aged leachate (>10 years) [3–5]. Generally, young landfill leachate has a high concentration of COD (>15,000 mg/L) and a high BOD_5/COD ratio (B/C > 0.6), and biological action can well remove organic and nitrogen-containing substances in leachate [6]. When the landfill life exceeds 10 years, most of the refractory organic matter in the leachate exists in the form of DOM composed of humus, which has higher aromaticity and molecular weight [7]. Due to the problems of non-compliance of anti-seepage measures in early garbage landfill, the aged landfill leachate migrates to the groundwater, causing serious pollution and threatening human health [8,9]. Therefore, the research and improvement of remediation technology of groundwater polluted by aged landfill leachate has important theoretical and practical application significance.

The aged leachate has poor biodegradability (B/C <0.1), implying biological treatment is ineffectiveness [10]. Therefore, physicochemical methods such as coagulation-flocculation, adsorption, membrane filtration and their combined process have been effectively applied [11–13]. However, the physicochemical method can only transfer the phase of pollutants, but not mineralize them. Meanwhile, it is expensive and easy to produce secondary pollution [14]. Therefore, it is urgent to find efficient and cost-effective alternative technology.

In recent researches, Advanced Oxidation Process (AOPs) have been widely used in different types of wastewater treatment due to their excellent degradation and mineralization effect on refractory organic matter [15]. At present, AOPs mainly include sulfate radical ($SO_4^{\bullet-}$) based advanced oxidation technologies (SR-AOPs) and hydroxyl radical ($^{\bullet}OH$) based advanced oxidation technologies (HR-AOPs). Compared with HR-AOPs, SR-AOPs have greater technology prospects. The reason is that $SO_4^{\bullet-}$ has higher redox potential (2.5–3.1 V vs 1.8–2.8 V) than $^{\bullet}OH$, adapts to a wider pH range, and has a longer half-life, which can

* Corresponding authors at: State Key Laboratory of Geohazard Prevention and Geoenvironment Protection, Chengdu University of Technology, Chengdu 610059, China
E-mail addresses: liaobing17@cdut.edu.cn (B. Liao), liuguo@cdut.cn (G. Liu).

https://doi.org/10.1016/j.apcatb.2021.120744
Received 24 June 2021; Received in revised form 30 August 2021; Accepted 19 September 2021
Available online 21 September 2021

mineralize organic pollutants in wastewater to a greater extent [16]. $SO_4^{\bullet-}$ can be obtained by energy radiation, alkali activation, or assisted catalytic activation of peroxymonosulfate (PMS) or peroxydisulfate (PDS) [17–20]. Both PMS and PDS have O-O bond, but PMS has an asymmetric structure and requires less energy to break the bond, so it is easier to be activated, and its oxidation efficiency is better than PDS, which has been widely concerned [21].

In recent years, metal and metal oxides (sulfides) have attracted extensive attention due to their good catalytic activity, low requirements for instruments and great potential for catalyst recovery and reuse in the process of PMS activation [21,22]. It has been shown that Cu-Fe bimetallic oxides ($CuFeO_2$ or $CuFe_2O_4$) activate PMS or PDS to degrade refractory organic compounds more efficiently than single metals because of the synergistic effect of transition metals Cu and Fe (Cu^+ can provide electrons to reduce Fe^{3+} to Fe^{2+}) [23,24]. In addition, Fan et al. found that S^{2-} can provide electrons to promote the cycle of Fe^{3+}/Fe^{2+}, thus realizing the efficient degradation of chloroaniline in FeS/PDS system [25]. It is worth noting that NCP is one of the most abundant and widely distributed copper deposits in the world, accounting for about 70% of the earth's copper, and the main component is $CuFeS_2$. Meanwhile, Nie et al. confirmed that the activation activity of hydrothermal synthesized $CuFeS_2$ on PMS is higher than that of Cu_2S, FeS_2, $CuFeO_2$ and Co_3O_4 [21]. If the natural mineral of chalcopyrite has similar catalytic properties, compared with the chemically synthesized $CuFeS_2$, NCP will reduce the complicated process of preparation, and become an efficient and cost-effective catalyst towards PMS for organic pollutant removal, greatly reduce the repair cost and increase the possibility of its use in in-situ remediation of groundwater polluted by refractory organic matter. Therefore, NCP has a certain practical significance in activating PMS to efficiently oxidize and degrade refractory organic pollutants.

In this study, a groundwater polluted by aged landfill leachate in an informal landfill was taken as the research object, and NCP was used as the activator of PMS. The influencing factors of remediation of polluted groundwater by NCP/PMS system were explored. The mechanism of activation of PMS by NCP and conversion of DOM in polluted groundwater were clarified. The toxicity test of the polluted groundwater before and after remediation was carried out by *Chlorella pyrenoidosa*. In addition, the sand column experiment was used to simulate the NCP/PMS remediation of groundwater polluted by aged landfill leachate. The study results provide data and theoretical support for in-situ remediation of groundwater polluted by refractory organic matter.

2. Materials and methods

2.1. Sample collection

The water samples were collected from the groundwater polluted by the aged landfill leachate of an informal landfill in Guangyuan City, Sichuan Province, China. Special sampling bottles were used for collection and kept at 4 °C in the refrigerator to reduce the biological content of the water samples. The groundwater polluted by aged landfill leachate is dark yellow, with a small amount of flocculent sediment, and odorless. The specific physical and chemical properties of the water samples are shown in Table 1. Furthermore, semivolatile organic compound and volatile organic compound in polluted groundwater were identified by gas chromatography-mass spectrometry (GC–MS, Agilent 7890) and purge-capture GC-MS (P&T-GC-MS, Agilent 7890), respectively. The test method refers to Water and Wastewater Testing and Analysis Methods (Fourth Edition) published by China Environmental Publishing Group. The results show that the main contaminants were phenols (phenol and its derivatives), phthalates (dibutyl phthalate) and polycyclic aromatic hydrocarbons (eg. naphthalene and anthracene), which manifest that the main organic matter in polluted groundwater is refractory organic matter and has great toxicity.

Table 1
The specific physical and chemical properties of the water samples.

Sample	pH	COD ($mg{\cdot}L^{-1}$)	TOC ($mg{\cdot}L^{-1}$)	UV_{254} (cm^{-1})	Chroma (CN)
Polluted groundwater	7.8 ± 0.2	321	156	3.974	0.192

2.2. Chemicals

Peroxymonosulfate (PMS, $KHSO_5{\cdot}0.5KHSO_4{\cdot}0.5\ K_2SO_4$) was purchased from Shanghai Aladdin Bio-Chem Technology Co., LTD. Other chemicals including sodium persulfate (PDS, $Na_2S_2O_8$), hydrogen peroxide (H_2O_2), ethanol (C_2H_5OH), tert-butyl alcohol (TBA), *p*-benzoquinone (BQ), *p*-hydroxybenzonic acid (*p*-HBA), benzoic acid (BA) and Nitrotetrazolium chloride blue (NBT), sulfuric acid (H_2SO_4) and sodium hydroxide (NaOH) were purchased from Chengdu Kelong chemical reagent company (Sichuan, China). All the above chemicals are of analytical grade and employed without further purification. Raw NCP ore was brought from Daye City, Hubei province, China. The raw ore was milled with an agate mortar and sieved (<150 μm). In order to better evaluate natural minerals, NCP was not pretreated in any other way.

2.3. Experimental procedure

2.3.1. Batch degradation experiments

All the experiments were performed in the 250 mL beaker and kept in a constant temperature water bath magnetic stirrer at 25 ± 2 °C. For each experiment, predetermined amounts of NCP and PMS were dispersed in 100 mL groundwater polluted by the aged landfill leachate with a mechanical stirrer (350 rpm). The initial pH of polluted groundwater was adjusted with 1 M H_2SO_4 or NaOH. During the reaction process, 3.0 mL sample was collected by 5.0 mL syringe, filtered immediately through 0.45 μm polyethersulfone (PES) filter head, and stored in a 5 mL centrifuge tube, which was quenched with 75 μL $Na_2S_2O_3$ (0.2 M) to quench the oxidation reaction. All experiments were performed with three parallel samples, the data in the figure are average values, and the error bars represent the standard deviation of the average value. In order to determine the active oxygen species in the NCP/PMS system, the quenching experiments were carried out by adding ethanol (100 mM), TBA (100 mM) and BQ (2.5 mM), which are scavengers of $SO_4^{\bullet-}$, $^{\bullet}OH$ and superoxide radical ($O_2^{\bullet-}$), respectively [26–28].

2.3.2. Parameter optimization

Response surface method (RSM) is a robust mathematical and statistical tool for optimizing experimental parameters and evaluating the interaction of key factors, which can be displayed by three-dimensional graphics or mathematical equations [29]. In this study, the Box–Behnken design (BBD) model in Design Expert (version 10) software was used to explore the impact of three key factors (initial pH, NCP dosage and PMS concentration) with 17 tests on TOC degradation efficiency. The relevant experimental data were analyzed in detail by using the Design Expert 10.0 software.

2.3.3. Column experiment

In order to investigate the remediation performance of NCP/PMS system for polluted groundwater under flowing condition, a vertical one-dimensional column experiment was carried out. The pretreatment of the experimental sand and the column packing process are detailed in Text S1. The schematic diagram of sand column experiment and the basic parameters of NCP/sand—filled column and sand—filled column are shown in Fig. S1 and Table S1, respectively. The polluted groundwater was mixed evenly with a certain amount of PMS (PMS

concentration is 25 mM) and pumped into the packed column from bottom up through a peristaltic pump at a flow rate of 1 mL/min (3 rpm). During the reaction, samples were taken from the upper end of the column at a predetermined time point, and $Na_2S_2O_3$ (0.2 M) was added to terminate the reaction. After filtering with a 0.45 μm PES filter, the concentration of TOC, Total Fe (TFe), Fe^{2+}, Total Cu (TCu), Cu^{2+} and PMS in the solution were measured.

2.4. Toxicity test

Aged landfill leachate is a kind of organic wastewater with high concentration and high toxicity. Although the toxicity of aged landfill leachate into groundwater has a certain reduction, it still has high biological toxicity. At the same time, organic compounds in polluted groundwater may produce more toxic intermediate products after advanced oxidation treatment. Therefore, the toxicity of polluted groundwater before and after the reaction were tested by *Chlorella pyrenoidosa*, which is a kind of algae widely existing in fresh water and seawater [30,31]. The inhibition of *Chlorella pyrenoidosa* growth can well reflect the potential ecological risk of treated wastewater entering natural water [32]. The methods of algae cultures, sample pretreatment, and toxicity test are shown in Text S2 in Supplementary Materials.

2.5. Characterization and analytical methods

The phase composition and crystal structure of NCP were detected by X-ray diffractometer (XRD, Cu Kα radiation (λ = 0.15418 nm), Shimadzu 6100, Japan). The qualitative and quantitative analysis of the elements in NCP were analyzed by X-ray fluorescence analyser (XRF-1800, Shimazu, Japan). Surface morphology, element composition and element distribution of NCP were examined via scanning electron microscopy (SEM, FEI Inspect F50, Thermo, USA), energy dispersive spectroscopy (EDS, K-Alpha, Thermo, USA), transmission electron microscopy (TEM, JEM-2100, JEOL) and TEM element scanning (TEM-mapping). The chemical valence states of key elements on the surface of NCP were determined by an X-ray photoelectron spectroscopy (XPS, JEM-2100, JEOL). Besides, Fourier transform infrared (FT-IR, Agilent Cary 660) spectra of NCP was used to identify the types of surface functional groups. The N_2 adsorption/desorption isotherms was analyzed by Autosorb iQ Station 1 (Quantachrome, USA) and the specific surface areas of NCP was calculated based on Brunauer-Emmett-Teller (BET) model.

The pH of the samples were measured by a pH meter (PHS-320, China). TOC of samples were measured by TOC analyzer (TOC-L CPH, Shimazu, Japan). The UV–vis absorption spectra of samples were performed in 10 mm quartz cuvettes by a UV–vis spectrophotometer (Alpha-1900S, Shanghai Puyuan Instrument Co., Ltd). During the reaction, the changes of DOM in the sample were measured by three-dimensional (3D-EEM) fluorescence spectroscopy with 10 mm quartz cuvette (optical path 10 nm, integration time 0.5 s) at the excitation-emission wavelengths (Ex/Em) = (230–550 nm/83–630 nm) and ultrapure water was used as the blank. TCu and TFe were detected by Atomic Absorption Spectrometer (GGX-9, Beijing Haiguang Co., Ltd). The concentrations of Fe^{2+} and Cu^{2+} were determined via 1,10-phenanthroline and dicyclohexanoneoxaly dihydrazone spectrophotometric method, respectively. The concentration of residual PMS was determined by potassium iodide ultraviolet spectrophotometry [33]. The chroma of polluted groundwater before and after treatment were characterized by color number (CN). The CN was determined using Eq. (1) [34,35], where A_{436}, A_{525} and A_{620} represent the absorbance of the sample at the wavelengths of 436, 525, and 620 nm, respectively.

$$CN = \frac{A_{436}^2 + A_{525}^2 + A_{620}^2}{A_{436} + A_{525} + A_{620}} \quad (1)$$

The reactive oxygen species ($SO_4^{\bullet-}$, $^{\bullet}OH$ and $O_2^{\bullet-}$) were detected by using electron spin resonance spectrometer (ESR, Bruker, USA) and 5,5-dimethyl-pyrroline N-oxide (DMPO) was used as the spin trapping agent [26]. After 60 s of reaction, the reactive oxygen species in the solution were determined by ESR. The concentration of common free radicals ($SO_4^{\bullet-}$, $^{\bullet}OH$ and $O_2^{\bullet-}$) in NCP/PMS system were quantified via high performance liquid chromatograph (HPLC) according to previous literature and *p*-HBA, BA and NBT were chosen as the indicators of $SO_4^{\bullet-}$, $^{\bullet}OH$ and $O_2^{\bullet-}$, respectively [36].

3. Results and discussion

3.1. Characterization

XRD pattern of NCP is shown in Fig. 1a. The NCP characteristic peaks observed at 2θ = 29.4°, 48.8°, 49.2°, 57.9° and 58.6°, which are consistent with the (112), (220), (204), (312) and (116) crystal planes of chalcopyrite (JCPDS 37–0471), and are also similar to the crystal form of magnetite $CuFeS_2$ nanoparticles prepared by Nie et al. [21], indicating that the main component of NCP is $CuFeS_2$. Significantly, a strong peak signal appears at 2θ = 26.6°, which is due to the presence of a certain amount of SiO_2 in NCP [37]. Except for this impurity peak, there are few impurity peaks in the XRD diffraction pattern, indicating that NCP has a high purity. Besides, Fe, Cu, S, Mg, Ca, Zn and Al are found by XRF analysis (Fig. 1b). The highest proportion of metallic elements is Fe, followed by Cu, which accounts for 27.3% and 24.2% of the total ore, respectively. Meanwhile, the proportion of S and Si in the mineral are more than 10%, accounting for 18.4% and 13.2% of the total ore, respectively. XRF results show that Cu, Fe and S are the main elements in NCP.

Fig. 1d gives the morphologies of the NCP. As can be observed, the shape and size of the NCP particles are different, and the surface is smoother. At the same time, the elements in the selected area in Fig. 1d were analyzed by energy dispersive spectrometer (EDS). As shown in Fig. 1e, the peaks of Cu, Fe and S are the most obvious, which indicate that Cu, Fe and S are the main chemical elements (i.e. Fe (33.2 wt%), Cu (29.5 wt%) and S (23.4 wt%) in NCP, which is consistent with the results of XRF. The partial TEM image of shows a typical microparticle with irregular shape. In addition, the distribution of Cu, Fe and S on the NCP surface were determined by TEM-mapping. From Fig. 1g to j, the two metals (Cu and S) are evenly distributed on the surface of the NCP, while S is concentrated locally. Moreover, to reveal the changes of NCP surface functional groups before and after the reaction, the FTIR spectrum is shown in Fig. 1c. The vibration peaks appear at 1024, 1120, 1624, and 3427 cm^{-1}, respectively. Among them, the peaks near 1024 cm^{-1} and 1624 cm^{-1} correspond to the Fe—CO and Fe—C═O stretching modes, respectively. And the peak near 1120 cm^{-1} corresponds to the Cu—CO stretching mode [38]. In the meantime, the peak near 3432 cm^{-1} can be attributed to the stretching vibration of the —OH group [39]. Comparing the FT-IR spectra of fresh and used NCP, it is found that the signals of used NCP are only enhanced at 1120 cm^{-1} (Cu—CO stretching) and 1024 cm^{-1} (Fe—CO stretching), indicating that metal ions (Cu^{2+}, Fe^{2+} or Cu^{+}) are adsorbed on the surface of NCP.

3.2. NCP/PMS degradation efficiency

At present, the most researched oxidants in advanced oxidation technology are PDS, PMS and H_2O_2. In order to reveal the remediation efficiency of NCP activated PDS, PMS and H_2O_2 on contaminated groundwater, seven control systems (three systems: NCP/PMS, NCP/PDS, NCP/H_2O_2; 4 separate NCP, PMS, PDS and H_2O_2 control groups) were designed with TOC and CN removal rate as evaluation indicators. Fig. 2a shows that the removal rates of TOC in polluted groundwater by NCP/PMS, NCP/PDS, NCP/H_2O_2, NCP, PMS, PDS and H_2O_2 within 120 min are 68.9%, 33.1%, 21.8%, 12.2%, 12.7%, 3.1% and 2.7%, respectively. The results show that the NCP/PMS system is significantly better than NCP/PDS, NCP/H_2O_2, NCP, PMS, PDS and H_2O_2 in

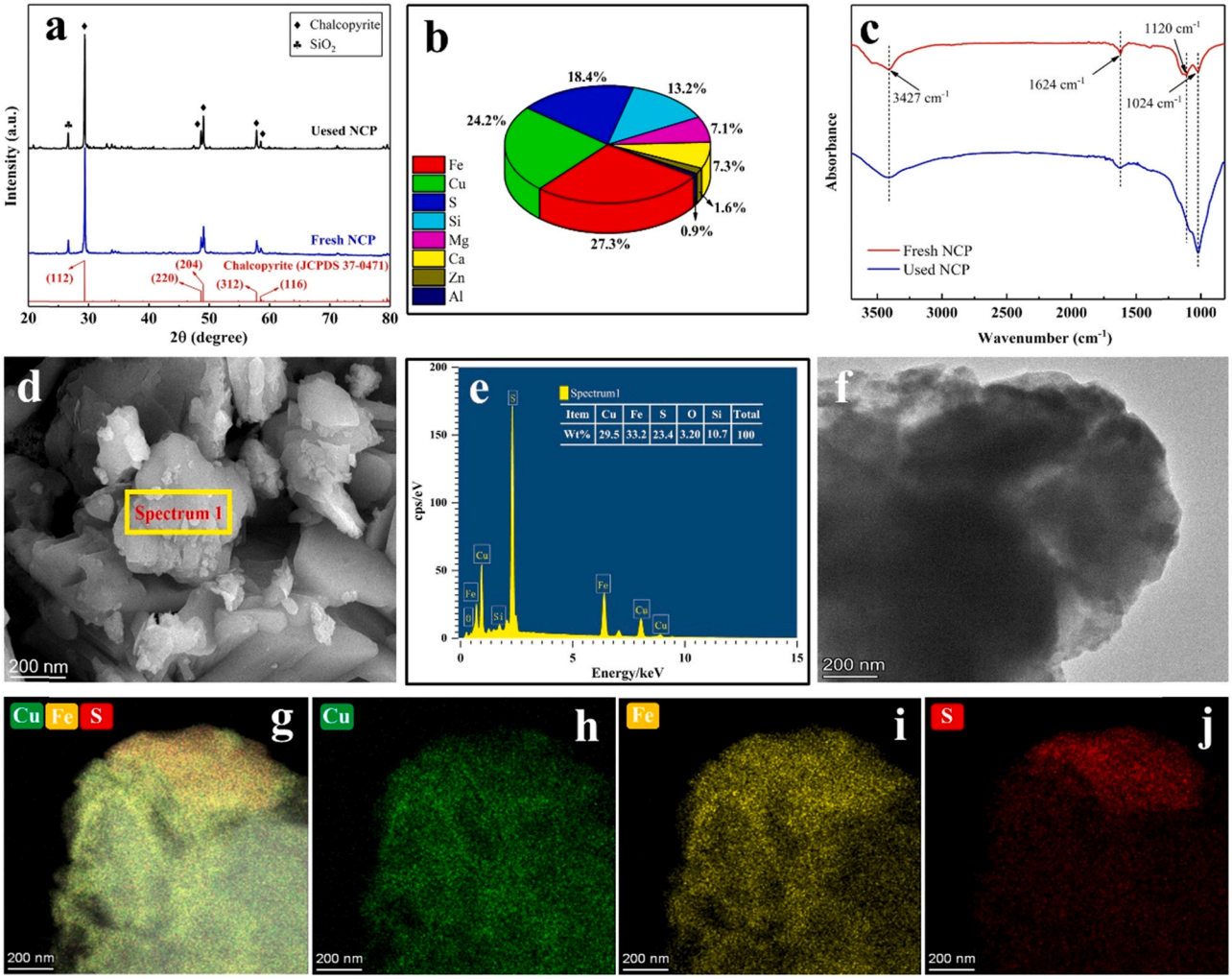

Fig. 1. (a) XRD pattern and (c) FT-IR spectra of the fresh and used NCP; (b) XRF pattern, (d) SEM image, (e) EDS, (f) TEM image and (g-j) TEM-mappings of the fresh NCP.

remediation of polluted groundwater. At the same time, it is worth noting that NCP alone also has a TOC removal rate of 12.2%, indicating that NCP has a certain adsorption performance. To better understand the adsorption performance of NCP, the surface area and pore volume were tested. From the N_2 adsorption/desorption isotherm of NCP (Fig. 2b), it can be seen that NCP has type IV isothermal characteristics, indicating that NCP is a mesoporous material [40]. The specific surface area and pore volume of NCP are calculated to be 8.2 m^2/g and 0.022 cm^3/g, respectively. Besides, the CN removal rate is also used as the evaluation index of the oxidation system. It can be clearly seen from Fig. 2a that the NCP/PMS system has a CN removal rate of 99% within 120 min, which is higher than other systems.

3.3. Effects of the key parameters of NCP/PMS process

3.3.1. Effect of NCP dosage

Fig. 2c shows the effect of different NCP dosages (1, 3, 5, 7, 10, 12 and 20 g/L) on the degradation efficiency of TOC in the NCP/PMS system. When there is no NCP in the reaction system, the removal rate of TOC is 17% (the result is shown in Fig. 2a). In contrast, when the NCP concentration is 1 g/L, the degradation efficiency of TOC is significantly increased to 31.9%, indicating that NCP can activate PMS to generate $SO_4^{\bullet-}$, thereby degrading organic matter in the solution. As the dosage of NCP increase from 1 g/L to 10 g/L, the degradation efficiency of TOC increase from 31.9% to 69.7%. This is mainly because as the dosage of NCP increase, the active sites of PMS also increase, thus generating more active species to enhance the degradation of TOC. However, with the increase of NCP dosage, the removal rate of TOC shows a downward trend, which may be because too much NCP will cover some of its own PMS active sites, thus reducing the performance of NCP in activating PMS.

3.3.2. Effect of PMS concentration

Fig. 2d shows the effect of different PMS concentrations (0, 4, 6, 8, 10, 20, 40, 60, and 80 mM) on the degradation efficiency of TOC in the NCP/PMS system. It can be seen that the TOC removal rate (35%) at 4 mM PMS concentration is significantly higher than that (8%) at 0 mM PMS concentration, which indicates that the adsorption of NCP on organic matter is very weak and PMS plays a key role in the degradation of TOC in solution. When the concentration of PMS increases from 4 mM to 20 mM, the removal rate of TOC rises from 35% to 70%. This is because higher PMS concentration helps more free radicals ($SO_4^{\bullet-}$, $^{\bullet}OH$ and $O_2^{\bullet-}$) are generated to promote the degradation of TOC in the solution [26]. However, when the dosage of PMS is further increased to 40 mM, the TOC removal rate shows a significant downward trend. On the one hand, excessive $SO_4^{\bullet-}$ will cause the self-scavenging reaction of $SO_4^{\bullet-}$ (Eq. (2)). On the other hand, the residual HSO_5^- will react with $SO_4^{\bullet-}$ (Eq. (3)), thereby reducing $SO_4^{\bullet-}$ concentration [41,42].

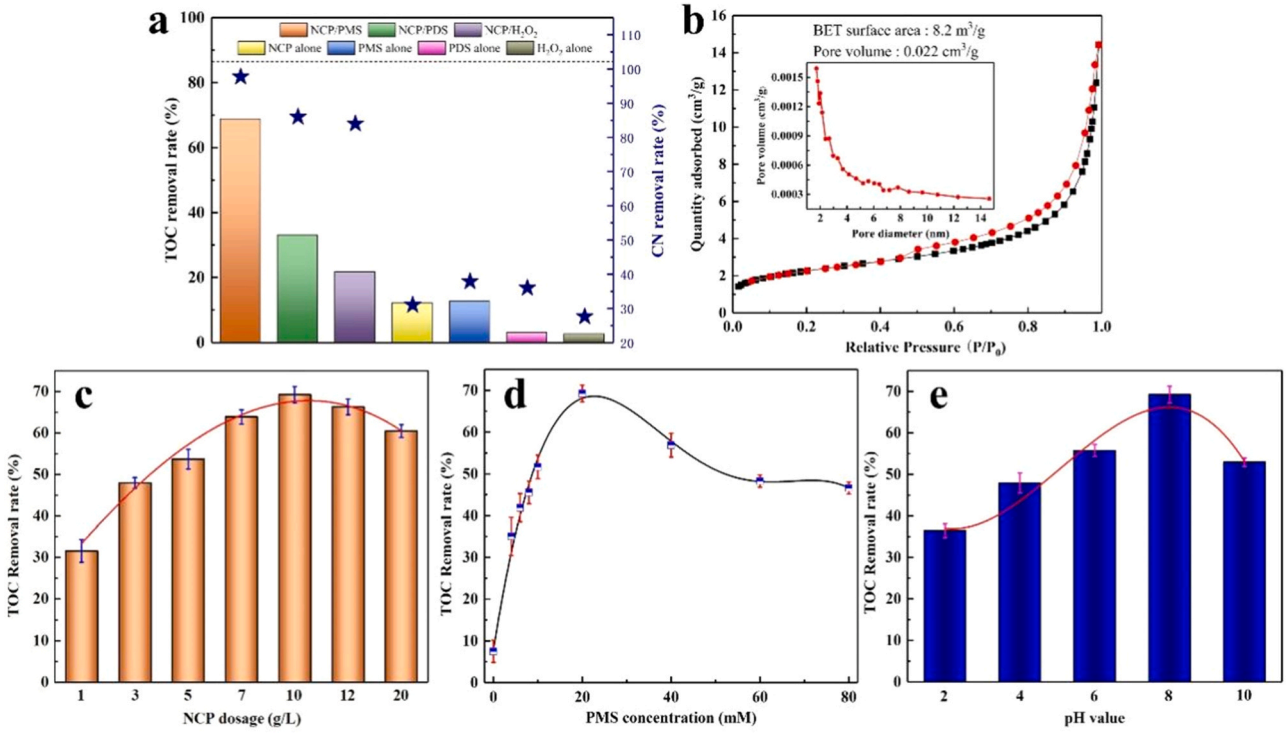

Fig. 2. (a) Performance of different systems for remediation of polluted groundwater; (b) adsorption/desorption isotherms of NCP and corresponding pore size distribution (inset). Effects of (c) NCP dosage, (d) PMS dosage, (e) pH changes on the degradation of TOC in NCP/PMS system.

$$SO_4^{\bullet-}+SO_4^{\bullet-}\rightarrow S_2O_8^{2-} \quad (2)$$

$$SO_4^{\bullet-}+HSO_5^{-}\rightarrow SO_5^{\bullet-}+SO_4^{2-}+H^+ \quad (3)$$

3.3.3. Effect of initial pH

In heterogeneous PMS oxidation system, the pH value of solution has an important influence on the formation of free radicals. In addition, pH value has a significant effect on the morphology of pollutants [26]. Therefore, the effects of different initial pH (2, 4, 6, 8 and 10) on the degradation efficiency of TOC in NCP/PMS system were studied. The results are shown in Fig. 2e.

It can be seen that the initial pH value has a significant effect on the degradation efficiency of TOC in polluted groundwater by NCP/PMS system. When the initial pH value is 8, the removal effect of TOC is the best, and the removal rate is about 70%, indicating that the weak alkali environment is conducive to the removal of TOC. When pH $<$ 8, the removal rate of TOC decreases with the decrease of pH, and the removal rate of TOC decreases by 15%, 20% and 35% at pH 6, 4 and 2, respectively. When pH $>$ 8, the removal rate of TOC decreases with the increase of pH, and the removal rate of TOC decreases by 18% when the pH is 10. When the solution is highly acidic, on the one hand, high concentration of H^+ will inhibit the hydrolysis of PMS, making it difficult for PMS to decompose and produce $SO_4^{\bullet-}$ [43]. On the other hand, CO_3^{2-} or HCO_3^- plasmas which have inhibitory effect on $SO_4^{\bullet-}$ in polluted groundwater are more likely to exist under acidic conditions, resulting in poor TOC removal effect in the system under acidic conditions [44]. However, when the solution is highly alkaline, Fe^{2+} on the surface of NCP is easy to form various stable iron substances (i.e. [$Fe(OH)_x$] and $Fe(OH)_2$) with OH^-, resulting in the failure of divalent iron [45]. At the same time, Fe^{3+} on the surface of NCP is easy to form $Fe(OH)_3$ precipitation with OH^- to cover the surface of NCP, thus blocking the activation of PMS by NCP.

3.4. Parameter optimization

3.4.1. Optimization results and model analysis of RSM

In order to obtain the optimal experimental conditions (i.e. pH value, NCP dosage and PMS concentration) of NCP activated PMS for remediation of polluted groundwater, RSM with the BBD model was used to optimize the experimental conditions and clarify the interactions among these variables. The results of Box-Behnken Design and corresponding response of TOC removal in the NCP/PMS system are shown in Table S2. Factor regression analysis was applied to the experimental data to express the final quadratic model by following the second-order polynomial equation, where the TOC removal rate (%) was expressed as the equation of initial pH (A), PMS concentration (B) and NCP dosage (C) (Eq. (4)).

$$\text{TOC removal efficiency (\%)} = 70{\cdot}94-10{\cdot}65A^2-6{\cdot}43B^2-7{\cdot}17\,C^2+13{\cdot}38AB-1{\cdot}54AC-0{\cdot}55BCE-1{\cdot}32\,A+4{\cdot}73B+4{\cdot}94\,C \quad (4)$$

The significance test and variance analysis were carried out for the multivariate quadratic regression equation (Table S3). As shown in Table S3, the computed Prob $>$ F of the model is less than 0.0001, and that of the lack-of-fit is 0.0178, which are much lower than 0.05, indicating that the fitted quadratic equation model is statistically significant [46]. It comprehensively shows that the quadratic regression equation model has a good fit in the design regression. In addition, from the perspective of three independent factors, for the response value TOC removal rate (%), the primary term C (NCP dosage), the secondary term A (initial pH), B (PMS concentration) and C (NCP dosage) have a significant impact on the response value. In summary, the significance of the effect on TOC removal rate is as follows: NCP dosage>PMS concentration>initial pH value. Table S4 also shows the R^2, adjusted R^2 (Adj R^2), coefficient of variation C.V.%, accuracy AP and predictive residual squared Press of the model. R^2 coefficient represents the change ratio of response value predicted by the model. The closer R^2 is to 1, the higher fitting degree of quadratic multinomial regression model is [47].

As can be seen from the table, both R^2 (0.9739) and Adj R^2 (0.9404) of the model are close to 1, which ensures that the quadratic model meets the experimental data. Meanwhile, the C.V.% of the fitting model is 4.11, which is much lower than 10, indicating that the fitting has high reliability [48]. In addition, the AP compares the range of predicted values of design points with the average prediction error, and a ratio greater than four indicates that the model has sufficient discrimination ability [48]. Fig. S2 shows the normal probability distribution of TOC removal parameters and the comparison between the predicted value and the actual value. Fig. S2a and b both show that the actual data is in good agreement with the data obtained by the model. In conclusion, the model fitted by BBD design is highly consistent with the actual experimental data.

The 3D response surface map can directly reflect the influence of multi-factor interaction on the response value, and more comprehensively optimize the analysis of experimental conditions. The 3D response surface map can directly find the optimal reaction conditions of each factor, while the contour shape reflects the interaction of each factor. The higher the degree of ellipsis, the more significant the interaction of the two factors is [47]. The response surface diagram of the influence of compound factors on TOC removal effect is shown in Fig. 3. It can be seen that the response curves of the three graphs all have obvious peaks, which means that there is a maximum response (i.e. optimal initial pH, PMS concentration and NCP dosage). Meanwhile, the contour maps corresponding to the three factors all have certain degree of ellipticity, and the interaction between NCP dosage and PMS concentration have the highest degree of ellipticity, indicating that the interaction between NCP dosage and PMS concentration have the greatest impact on the removal rate of TOC. And the optimal conditional of RSM fitting is shown in Table S5. According to the optimal experimental conditions, the predicted TOC removal rate is 71.5%. In conclusion, the initial pH, the concentration of PMS and the dosage of NCP have obvious interaction on the TOC removal rate.

3.4.2. Model validation

Based on the results of RSM and for the convenience of experimental operation, the economic optimal and the best conditions for the remediation of polluted groundwater by NCP/PMS are selected: pH = 8, PMS concentration 25 mM and NCP dosage of 10 g/L. In order to verify the validity and practicability of RSM regression model, three groups of experiments were carried out under the optimal experimental conditions with the same batch of water samples, and the corresponding reaction dynamics simulation were carried out (Fig. 4a). After 120 min, the TOC removal rates of the three groups of experiments are 69.91% 70.55% and 73.09%, respectively. The maximum relative error between the experimental values and the predicted values of the three times is less than 5%, indicating that the model has a good prediction effect on the experimental results, which has a certain guiding significance. At the same time, $Ln(TOC_0/TOC_t)$ is used to perform a kinetic fitting for time t. From the inset in Fig. 4a, it can be seen that the kinetics conforms to the second-order kinetic fitting, and the reaction rate constant is 0.038 g/(mg·min), the reaction has the fastest degradation rate within 30 min, the removal rate of TOC reaches 55%, and gradually becomes flat after 30 min, with only 15% TOC removal rate in 90 min. In addition, the pH and CN of the effluent at each time point were monitored. As shown in Fig. 4b, the pH drops from 8 to 5.3 within 5 min, which is due to the large amount of H^+ produced by PMS hydrolysis [43]. Besides, the degradation rate of CN in polluted groundwater by NCP/PMS system

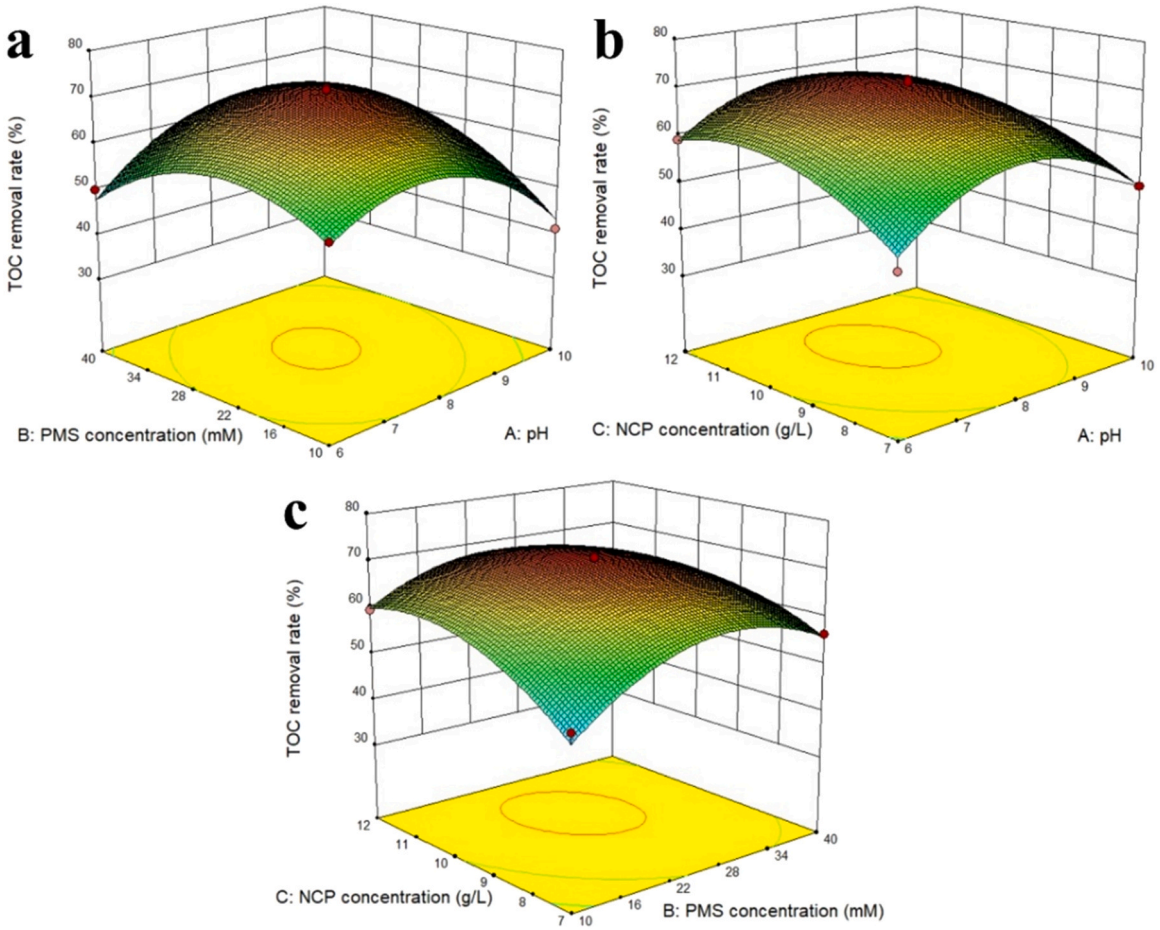

Fig. 3. Response surface graph of the effect of composite factors on TOC removal.

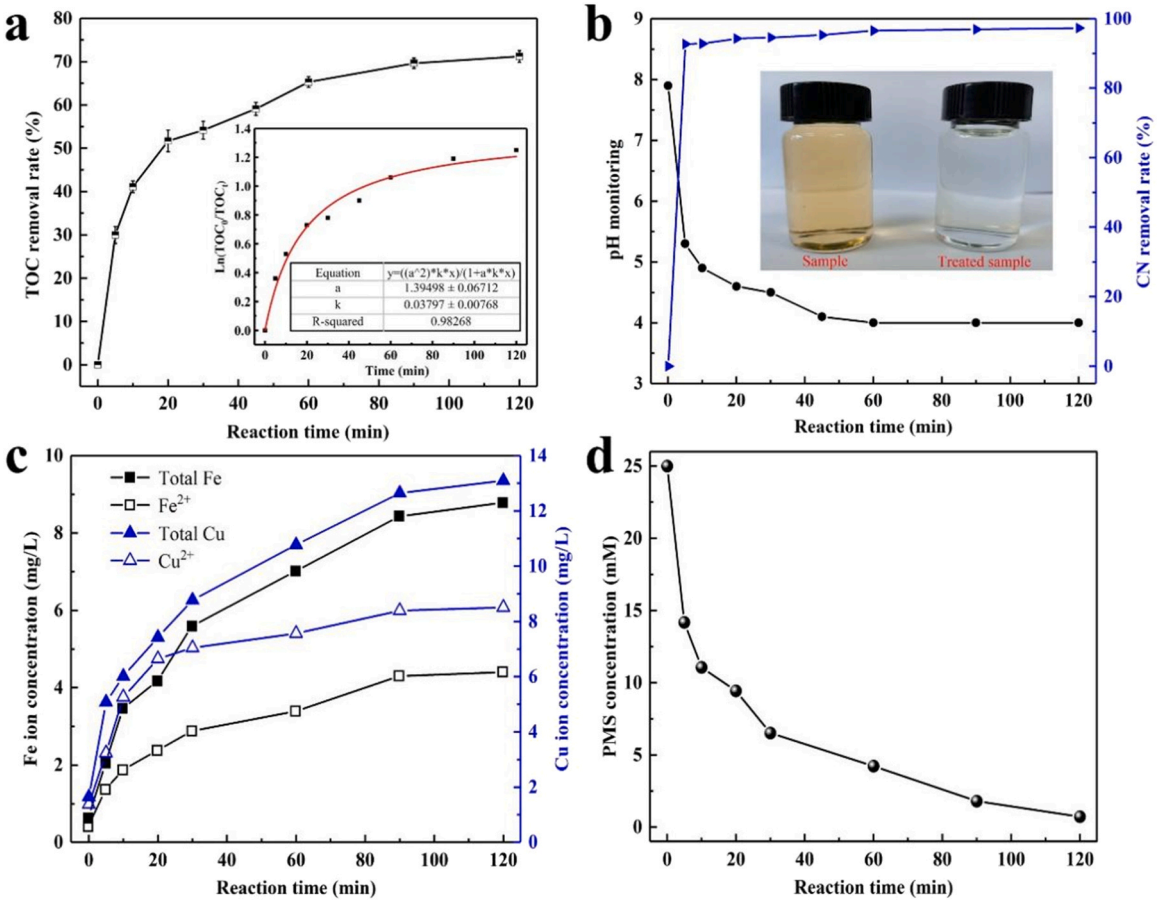

Fig. 4. (a) The degradation efficiency and kinetics of organic compounds in NCP/PMS system (inset) and (b) monitoring of effluent pH and removal efficiency of CN under the optimal reaction conditions; the changes of (c) TFe, Fe^{2+}, TCu and Cu^{2+} concentration, and (d) PMS concentration under optimal reaction conditions in the NCP/PMS system.

reaches 100% within 120 min, which is confirmed by the color change of polluted groundwater before and after remediation in Fig. 4b.

The concentrations of TFe, Fe^{2+}, TCu and Cu^{2+} in the solution at each reaction time point were monitored under the optimal experimental conditions (initial pH 8, PMS concentration 25 mM and NCP dosage 10 g/L). It can be seen from Fig. 4c that the rising trend of TFe and TCu concentration in the solution is roughly the same, the rising trend is gentle after 90 min, and the final concentration are 8.78 and 13.09 mg/L, respectively. The concentration of Cu^{2+} increases to the maximum (6.64 mg/L) in the first 20 min, and only increases by 1.87 mg/L in the next 100 min, while the concentration of Fe^{2+} increases gently in 120 min, and the final concentration is 4.40 mg/L. Therefore, Cu^{2+} dominates the whole reaction process, and the concentration of Cu^{+} increases gradually after 30 min. The concentrations of Fe^{2+} and Fe^{3+} are approximately the same. In addition, PMS concentration in the reaction process was monitored (Fig. 4d). As can be seen from the figure, PMS concentration is approximately 0 mg/L at 120 min, indicating that PMS is well activated by NCP. Notably, the concentration of PMS decreases sharply in the first 30 min, which may be due to the good activation property of NCP, which is consistent with the trend of TOC degradation rate rising rapidly in the first 30 min in Fig. 4a.

3.5. Possible mechanism of NCP activation of PMS

The literatures have shown that the initial pH of the solution has a certain influence on the generation of different free radicals [26,28,49,50]. Therefore, the species of free radicals in NCP/PMS system with different initial pH were identified by free radical quenching experiment. As can be seen from Fig. 5a, the degradation efficiency of TOC in polluted groundwater is reduced after the addition of the three quenching agents, indicating that $O_2^{\bullet-}$, $^{\bullet}OH$ and $SO_4^{\bullet-}$ are all generated in NCP/PMS system with different initial pH. Concurrently, different quenchers have different inhibitory effects on TOC removal rate, which also indicates that the initial pH of different solutions has a certain effect on the generation of three free radicals. In four NCP/PMS systems with different initial pH, compared with adding EtOH and TBA, adding BQ has less effect on the removal rate of TOC, which shows that $O_2^{\bullet-}$ has a relatively weak inhibitory effect on TOC degradation and $^{\bullet}OH$ and $SO_4^{\bullet-}$ play a major role in the system. It is worth noting that when the initial pH is 8, the removal rates of TOC are reduced by 65% and 60% respectively by adding EtOH and TBA. Compared with other pH (2, 5 or 11), the inhibition effect of EtOH on TOC degradation is more obvious, indicating that the production of $^{\bullet}OH$ and $SO_4^{\bullet-}$ at pH 8 is higher than other initial pH. Therefore, when the initial pH of the solution is 8, it is more conducive to the generation of three free radicals and can more effectively degrade TOC in the groundwater. To further quantify the concentration of common free radicals ($O_2^{\bullet-}$, $^{\bullet}OH$, $SO_4^{\bullet-}$) at each time point in the NCP/PMS system with initial pH 8, NBT, BA and p-HBA were used as $O_2^{\bullet-}$ [51], $^{\bullet}OH$ [52] and $SO_4^{\bullet-}$ [53] indicators. As shown in Fig. 5b, the concentration of $O_2^{\bullet-}$ gradually increases with the increase of time in the first 60 min, and stabilizes at 100 μM from 60 min. At the same time, the concentration of $O_2^{\bullet-}$ is lower than that of $^{\bullet}OH$ and $SO_4^{\bullet-}$ at each reaction time point, indicating that $O_2^{\bullet-}$ do not play a major role in the reaction process. In addition, the concentration of $^{\bullet}OH$ and $SO_4^{\bullet-}$ increase with the increase of reaction time, indicating that $^{\bullet}OH$ and $SO_4^{\bullet-}$ are produced continuously in the whole reaction process.

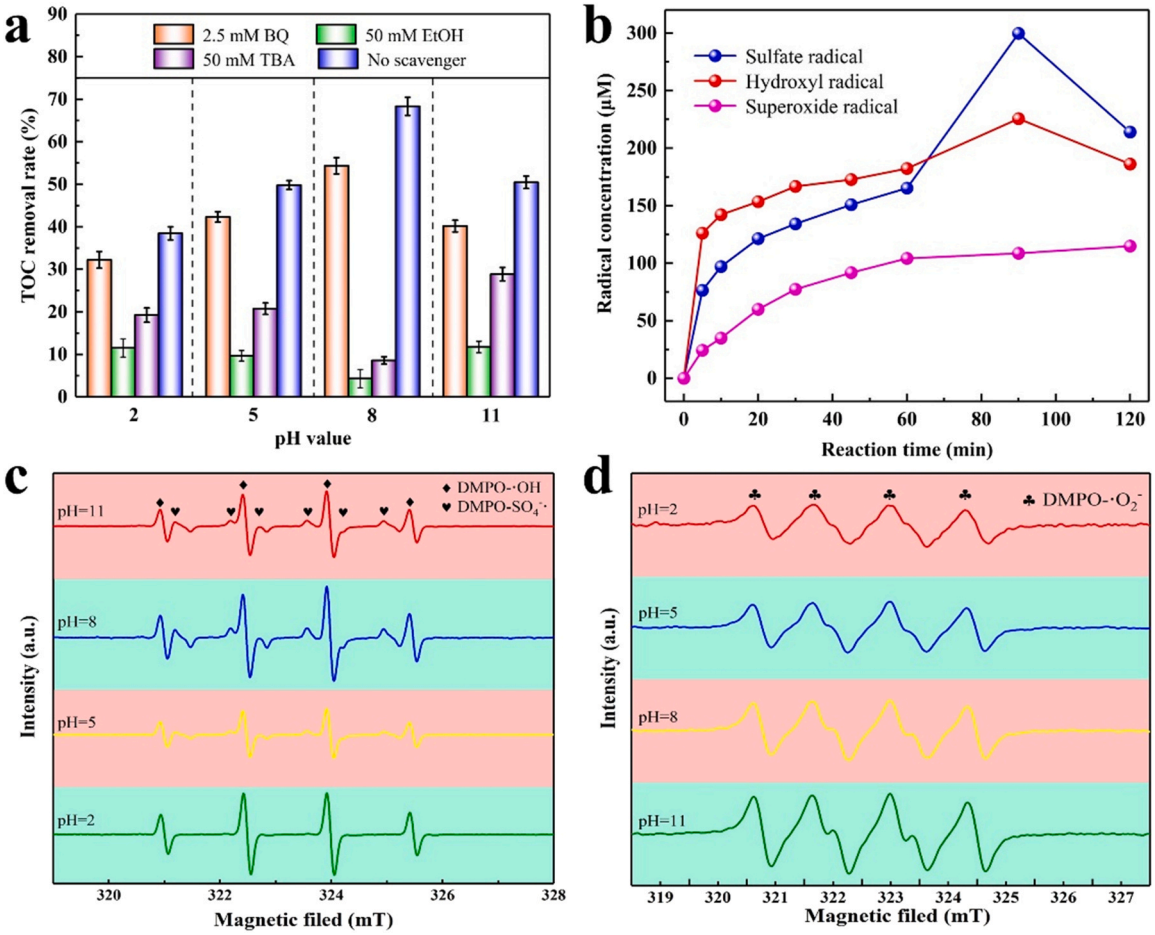

Fig. 5. (a) The quenching effect of different quenching agents on TOC degradation under different initial pH conditions; (b) the concentration change of $O_2^{\bullet-}$, $^{\bullet}OH$ and $SO_4^{\bullet-}$ formed in the NCP/PMS system at pH 8; (c) and (d) ESR spectra of NCP/PMS system under different initial pH conditions.

Meanwhile, the concentration of $^{\bullet}OH$ is higher than $SO_4^{\bullet-}$, which may be due to the conversion of $SO_4^{\bullet-}$ to $^{\bullet}OH$. With the increase of time, the concentration of $SO_4^{\bullet-}$ exceeds $^{\bullet}OH$, and reaches the maximum concentration (299.65 μM) at 90 min. After 90 min, the concentrations of $^{\bullet}OH$ and $SO_4^{\bullet-}$ decrease, which indicate that the reaction gradually weaken after 90 min. In summary, when the initial pH of the NCP/PMS system is 8, $^{\bullet}OH$ and $SO_4^{\bullet-}$ play an important role in the degradation of TOC.

In order to further verify the generation of three free radicals during the oxidation reaction process with different initial pH values, ESR spectra was used to test. As shown in Fig. 5c, the signals of DMPO — $^{\bullet}OH$ adduct (hyperfine coupling constant aN = aH = 1.49 mT) are observed at four initial pH. The peak height ratio of the four characteristic peaks of the DMPO — $^{\bullet}OH$ adduct is 1:2:2:1. Simultaneously, the signals of DMPO — $SO_4^{\bullet-}$ adduct (hyperfine coupling constants aN = 1.38 mT, aH = 1.01 mT, aH = 0.14 mT, aH = 0.79 mT) are observed at initial pH 5, 8 and 11. In addition, the signal of DMPO — $SO_4^{\bullet-}$ adduct is obviously weaker than that of DMPO — $^{\bullet}OH$ adduct, which may be related to the rapid conversion of $SO_4^{\bullet-}$ and $^{\bullet}OH$ and Eq. (5) illustrates the conversion relationship between the them [54]. When the initial pH is 8, the signals of DMPO — $SO_4^{\bullet-}$ and DMPO — $^{\bullet}OH$ adduct are stronger than those of other pH values, indicating that this pH environment is more conducive to the generation of $^{\bullet}OH$ and $SO_4^{\bullet-}$. Furthermore, the signals of DMPO-$O_2^{\bullet-}$ adduct (aN = 1.35mT, aH = 0.77mT) are found in NCP/PMS systems with different initial pH (Fig. 5d), and the signal intensity of adduct is similar, indicating that the initial pH has little effect on the generation of $O_2^{\bullet-}$. The ESR results are consistent with the quenching experiment, indicating that $O_2^{\bullet-}$, $^{\bullet}OH$ and $SO_4^{\bullet-}$ are produced under different initial pH conditions. However, compared with the initial pH of 2, 5 and 11, the initial pH of 8 is more favorable for the NCP/PMS system to produce $^{\bullet}OH$, $SO_4^{\bullet-}$, and the initial pH of 8 is close to the actual pH of the polluted groundwater, which is more conducive to the experiment.

$$H_2O+SO_4^{\bullet-}\rightarrow H^+ + SO_4^{2-} + {}^{\bullet}OH \quad (5)$$

Furthermore, to explore the mechanism of NCP activation of PMS, XPS measurements of NCP after reaction were carried out to reveal the changes of surface element composition and valence state of NCP before and after reaction. The survey XPS spectrum of NCP is shown in Fig. 6a. It can be seen that there are Fe2p, Cu2p, S2p, and O1s on the surface of NCP, which correspond to the characteristic peaks at 713.1, 932.1, 162.1, and 533.1 eV, respectively. The detected C and O may be due to the adsorption of amorphous C and O in air, and some non-metallic and metallic (e.g. Si and Al) oxides on the surface of NCP. The XPS spectra further confirms that the main elements in NCP are Fe, Cu and S. Compared with the full spectrum of XPS spectra of fresh and used NCP, it can be found that the Cu, O and S on the surface of NCP are significantly reduced, which may be due to the dissolution of metal oxygen (sulfur) compounds. To analyze the valence states of the main elements Cu, Fe, and S on the surface of the NCP more clearly and in detail, the high-resolution XPS spectra of Cu, Fe, and S were peak-fitted (Fig. 6b, c and d). The high-resolution Cu2p spectra of fresh and used NCP (Fig. 7b) show two strong peaks of $Cu2p_{1/2}$ and $Cu2p_{3/2}$ at 951.9 and 932.1 eV, respectively. No obvious satellite peaks are observed, which indicates that the valence state of Cu on the surface of fresh and used NCP is mainly +1 [21]. Copper hydroxide is usually produced by oxidation on

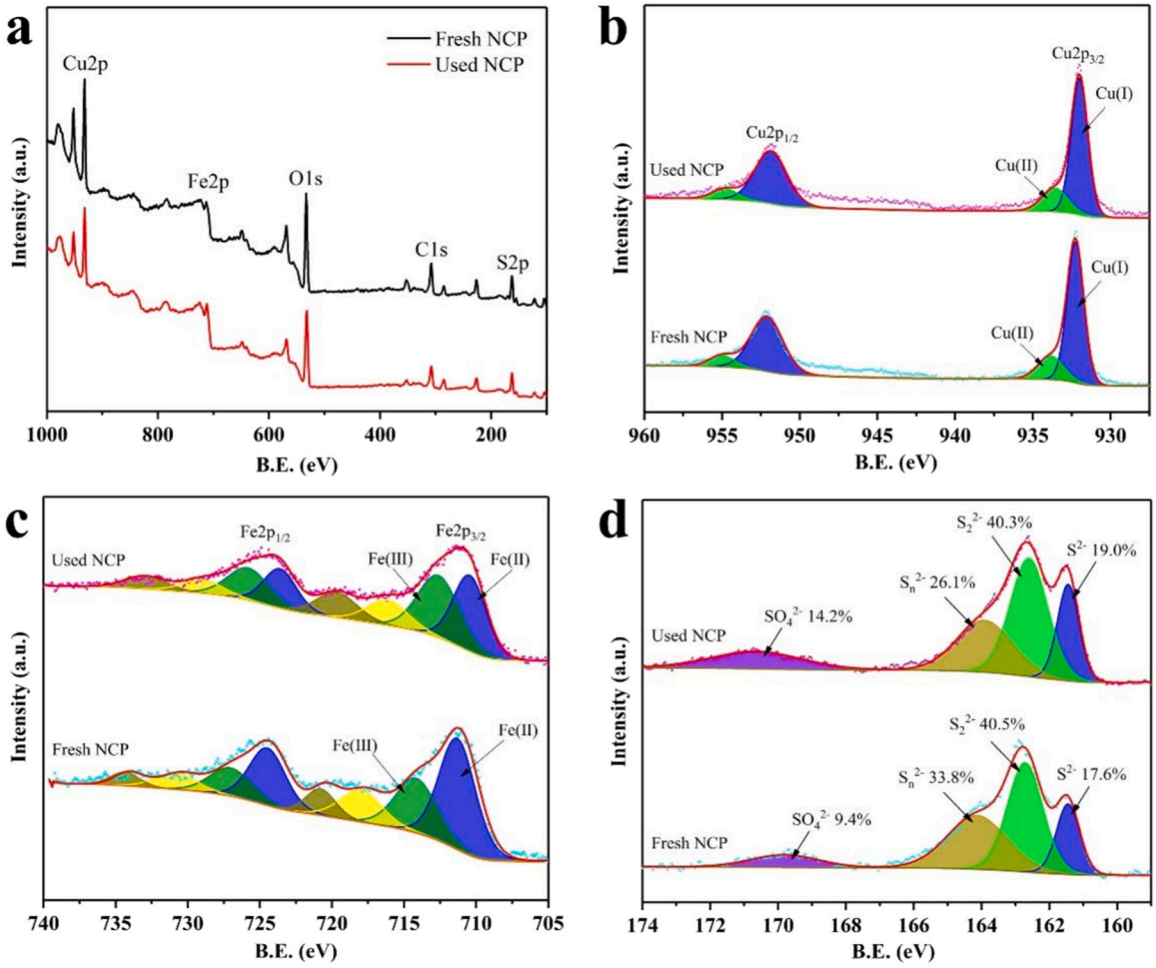

Fig. 6. XPS spectra of NCP before and after the reaction: (a) survey spectrum; (b) Cu 2p, (c) Fe 2p and (d) S 2p spectra.

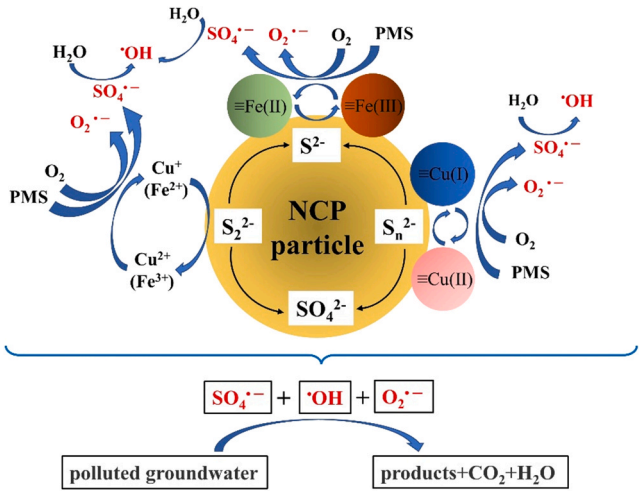

Fig. 7. Schematic diagram for the activation mechanism of PMS by NCP.

the surface of NCP, and copper exists in the form of Cu^{2+}, so the peaks at 934.3 and 954.3 eV correspond to $Cu2p_{3/2}$ and $Cu2p_{1/2}$ of Cu^{2+}, respectively [55]. Fig. 6c shows the high-resolution Fe2p spectra of fresh and used. After the reaction is completed, the peak positions of used NCP are similar to that of fresh NCP. There are two peaks at 714.4 and 711.5 eV, corresponding to $Fe2p_{1/2}$ and $Fe2p_{3/2}$, respectively, which are characteristic peaks of Fe^{2+} and Fe^{3+} [25,56,57]. By peak fitting, it is found that the proportion of Fe^{2+} species on the surface of NCP decreases significantly after the reaction, while the proportion of Fe^{3+} species increases, indicating that Fe^{2+} is oxidized to Fe^{3+} on the surface of NCP. The high-resolution S2p spectra of fresh and used NCP are shown in Fig. 6d. The four main peaks are respectively located at 161.2, 162.4, 163.9 and 169.1 eV, which correspond to S^{2-} [58], S_2^{2-} [57], S_n^{2-} [59] and SO_4^{2-} [25], respectively. The percentages of S^{2-}, S_2^{2-}, S_n^{2-} and SO_4^{2-} species on the surface of the fresh NCP catalyst are 17.6%, 40.5%, 33.8% and 9.4%, respectively. After the reaction, the percentages of S^{2-} and SO_4^{2-} species respectively increase to 19.0% and 14.2%, while the proportions of S_n^{2-} decrease significantly, indicating that S_n^{2-} was transformed into S^{2-}, S_2^{2-} and SO_4^{2-} species in the oxidation process. Additionally, some studies have also reported that sulfur species (S^{2-}, S_2^{2-}, and S_n^{2-}) play a key role in promoting the reduction cycles of Cu^{2+}/Cu^{+} and Fe^{3+}/Fe^{2+} [21,26,60]. In a sense, XPS results of S also show that S_n^{2-}, as electron donors, can participate in the Fe^{3+}/Fe^{2+} and Cu^{2+}/Cu^{+} cycles in the NCP/PMS system, resulting in a change in the proportion of four sulfur species.

Based on the above results and discussion, Fig. 7 shows the possible activation mechanism of PMS in the NCP/PMS system. First, the metal ions (Cu^{+} and Fe^{2+}) release by the NCP into the solution and the metal fixed on the surface of the NCP (≡Cu(I) or ≡Fe(II)) activate O_2 and PMS to produce $O_2^{\bullet-}$ and $SO_4^{\bullet-}$, respectively. They are oxidized to Cu^{2+}, Fe^{3+}, ≡Cu(II) and ≡Fe(III) (Eq. (6)~(9)) [61]. In the meantime, $SO_4^{\bullet-}$ further oxidizes H_2O to $^{\bullet}OH$ (Eq. (10)) [28], and $SO_4^{\bullet-}$ can be converted to $^{\bullet}OH$ (Eq. (11)) [62]. In addition, Fe^{3+} and Cu^{2+}, ≡Fe (III) and ≡Cu (II) are reduced to Fe^{2+}, Cu^{+}, ≡Fe (II) and ≡Cu (I) by sulfur species S^{2-}, S_2^{2-} and S_n^{2-} on the surface of NCP (Eqs. (12)-(17)) [25]. Besides, the

regeneration of Fe^{2+} can also be achieved by transferring electrons from Cu^{+} to Fe^{3+} (Eq. (18)). The regenerated Cu^{+}, Fe^{2+}, ≡Cu (I) and ≡Fe (II) can reactivate PMS and continuously generate $SO_4^{\bullet -}$, $^{\bullet}OH$ and $O_2^{\bullet -}$, resulting in macromolecular refractory organic compounds in polluted groundwater are degraded to small organic compounds, and some organic compounds are completely oxidized to CO_2 and H_2O.

$$HSO_5^- + Cu^+(Fe^{2+}) \rightarrow Cu^{2+}(Fe^{3+}) + SO_4^{\bullet -} + SO_4^{2-} \quad (6)$$

$$O_2 + Cu^+(Fe^{2+}) \rightarrow Cu^{2+}(Fe^{3+}) + O_2^{\bullet -} \quad (7)$$

$$HSO_5^- + \equiv Cu(I)(\equiv Fe(II)) \rightarrow \equiv Cu(II)(\equiv Fe(III)) + SO_4^{\bullet -} + SO_4^{2-} \quad (8)$$

$$O_2 + HSO_5^- + \equiv Cu(I)(\equiv Fe(II)) \rightarrow \equiv Cu(II)(\equiv Fe(III)) + O_2^{\bullet -} \quad (9)$$

$$H_2O + SO_4^{\bullet -} \rightarrow {}^{\bullet}OH + H^+ + SO_4^{2-} \quad (10)$$

$$SO_4^{\bullet -} + OH^- \rightarrow {}^{\bullet}OH + SO_4^{2-} \quad (11)$$

$$S^{2-} + Cu^{2+}(Fe^{3+}) \rightarrow Cu^+(Fe^{2+}) + S_2^{2-} \quad (12)$$

$$S^{2-} + \equiv Cu(II)(\equiv Fe(III)) \rightarrow \equiv Cu(I)(\equiv Fe(II)) + S_2^{2-} \quad (13)$$

$$S_2^{2-} + Cu^{2+}(Fe^{3+}) \rightarrow Cu^+(Fe^{2+}) + S_n^{2-} \quad (14)$$

$$S_2^{2-} + \equiv Cu(II)(\equiv Fe(III)) \rightarrow \equiv Cu(I)(\equiv Fe(II)) + S_n^{2-} \quad (15)$$

$$S_n^{2-} + Cu^{2+}(Fe^{3+}) \rightarrow Cu^+(Fe^{2+}) + SO_4^{2-} \quad (16)$$

$$S_n^{2-} + \equiv Cu(II)(\equiv Fe(III)) \rightarrow \equiv Cu(I)(\equiv Fe(II)) + SO_4^{2-} \quad (17)$$

$$Cu^+ + Fe^{3+} \rightarrow Cu^{2+} + Fe^{2+} \quad (18)$$

3.6. Conversion of dissolved organic pollutants

The concentration, aromaticity and complexity of organic matter in wastewater often determine the absorption intensity of UV–vis spectrum, so UV–vis spectrum was often used to characterize the changes of organic matter concentration and molecular structure in wastewater [63]. As shown in Fig. S3, the UV–vis absorption intensity of the polluted groundwater is relatively high, which indicates that the polluted groundwater has high content of organic matter, high aromatic humus, and most of them are conjugated systems. It is worth noting that the absorption of ultraviolet light in the polluted groundwater decreases significantly after 30 min reaction in the NCP/PMS system, and shows a trend of gradual decline after 30 min reaction. It is speculated that NCP has good activation performance on PMS in the first 30 min, and produces a large amount of $^{\bullet}OH$ and $SO_4^{\bullet -}$, which makes the macromolecular organic matter (humic acid) in the polluted groundwater greatly destroyed and mineralized. With the increase of reaction time, the activation performance of NCP and the amount of PMS decrease, leading to the reduction of reaction efficiency. This indicates that after the NCP/PMS system treatment of polluted groundwater, the macromolecular structure of organic matter is destroyed, and the aromaticity and complexity are significantly reduced.

At a specific wavelength, the ratio of UV–vis absorbance can usually reflect the structural characteristics of different organics. Among them, the indicators E_{240}/E_{420} and E_{300}/E_{400} are widely used, and E_{240}/E_{420} and E_{300}/E_{400} respectively indicate the degree of humus structure and molecular weight polymerization. The ratio is negatively correlated with the degree of structure of humus and the degree of molecular weight polymerization of organic matter [64,65]. As can be seen from Table S6, the values of E_{240}/E_{420} and E_{300}/E_{400} both increase with the extension of reaction time. After 120 min reaction in NCP/PMS system, the values of E_{240}/E_{420} and E_{300}/E_{400} both increase by 395.06 and 23.73 compared with 54.94 and 4.840 of raw water, indicating that the structure degree, molecular weight and condensation degree of organic matter and humic acid in polluted groundwater are all reduced. At the same time, E_{280} and E_{254} are used as the indexes of the content of aromatic, hydrophobic and unsaturated organic compounds in the polluted groundwater, respectively, and they are all in direct proportion to their ratios. As shown in Table S6, the values of E_{280} and E_{254} both decrease with the extension of time, indicating that NCP/PMS system can reduce the aromaticity and hydrophobicity of organic matter in polluted groundwater and reduce the content of unsaturated organic matter. Therefore, NCP/PMS system has good degradation and mineralization performance for organic matter in polluted groundwater.

Groundwater polluted by aged landfill leachate contains a variety of organic compounds, which are mainly composed of humic acid (HA), rich acid (HF), hydrophilic organic acids, amino acids, carbohydrates, polycyclic aromatic hydrocarbons and other substances. Most of them are conjugated double-bond aromatic hydrocarbons or conjugated structural substances containing double bond, carboxyl group and other groups. All of these substances have different luminescent regions in the three-dimensional fluorescence spectrum [66]. Therefore, the composition of pollutants in polluted groundwater and their transformation characteristics during the degradation process can be inferred from the three-dimensional fluorescence distribution map, and the biodegradability before and after the remediation of polluted groundwater can be analyzed according to the removal of fulvic acid substances in the ultraviolet region. According to the type and location of the fluorescent substances, the fluorescence spectrum can be divided into five regions: aromatic protein I (region I: Ex < 250 nm, Em < 330 nm); aromatic protein II (region II: Ex < 250 nm, 330 nm < Em < 380 nm); fulvic acid (zone III: Ex < 250 nm, Em > 380 nm); byproducts of microbial metabolism (zone IV: Ex > 250 nm, Em < 380 nm) and humic acid (zone V: Ex > 250 nm, Em > 380 nm) [67].

Under the conditions of initial pH of 8, PMS concentration of 25 mM and NCP dosage of 10 g/L, three-dimensional fluorescence spectrum scanning was carried out on the polluted groundwater at different reaction time points to analyze the change trend of organic matter. The scanning results are shown in Fig. 8. As shown in Fig. 8 (0 min), the three-dimensional fluorescence spectrum luminescence area of groundwater polluted by aged landfill leachate is mainly located in the by-products of microbial metabolism IV area and humic acid-like V area, of which humic acid-like is the main component. Concurrently, there are two main luminescence regions in these two regions, namely F1 (Ex/Em = 240–260 nm/430–470 nm) and F2 (Ex/Em = 275–475 nm/360–610 nm). Among them, F1 is the fluorescence peak of fulvic acid in the ultraviolet region, which is mainly caused by organic substances with low molecular weight and high fluorescence efficiency, usually representing fulvic acid. F2 is the fluorescence peak of fulvic acid in the visible region, which is mainly produced by relatively stable aromatic substances with high molecular weight and usually represents humic acid [68]. Moreover, the fluorescence intensity in the visible light region of the wastewater is high, which indicates that the groundwater polluted by aged landfill leachate can represent the typical refractory wastewater [69].

Furthermore, it can be clearly seen from Fig. 8 (30 min) that after 30 min treatment with NCP/PMS system, the fluorescence peak F1 of fulvic acid in the ultraviolet region is almost not displayed, indicating that this part of the organic matter has been well removed. In the interim, the peak intensity of the fluorescence peak of fulvic acid in the visible area is also significantly reduced and the removal rate of fulvic acid reaches 55.95% within 30 min. As time goes by, the peak intensity of fulvic acid gradually decreases, and the final removal rate is 92.96% (Table S7). Most notably, the fluorescence peak position of fulvic acid in the visible region of wastewater after NCP/PMS treatment has a blue shift (Ex/Em shifted from 365/443 nm to 330/410 nm), which indicates that the oxidation rate of refractory humic acid in wastewater is accelerated, the molecular structure of humic acid is destroyed, and the degree of condensation of organic molecules is greatly reduced [69].

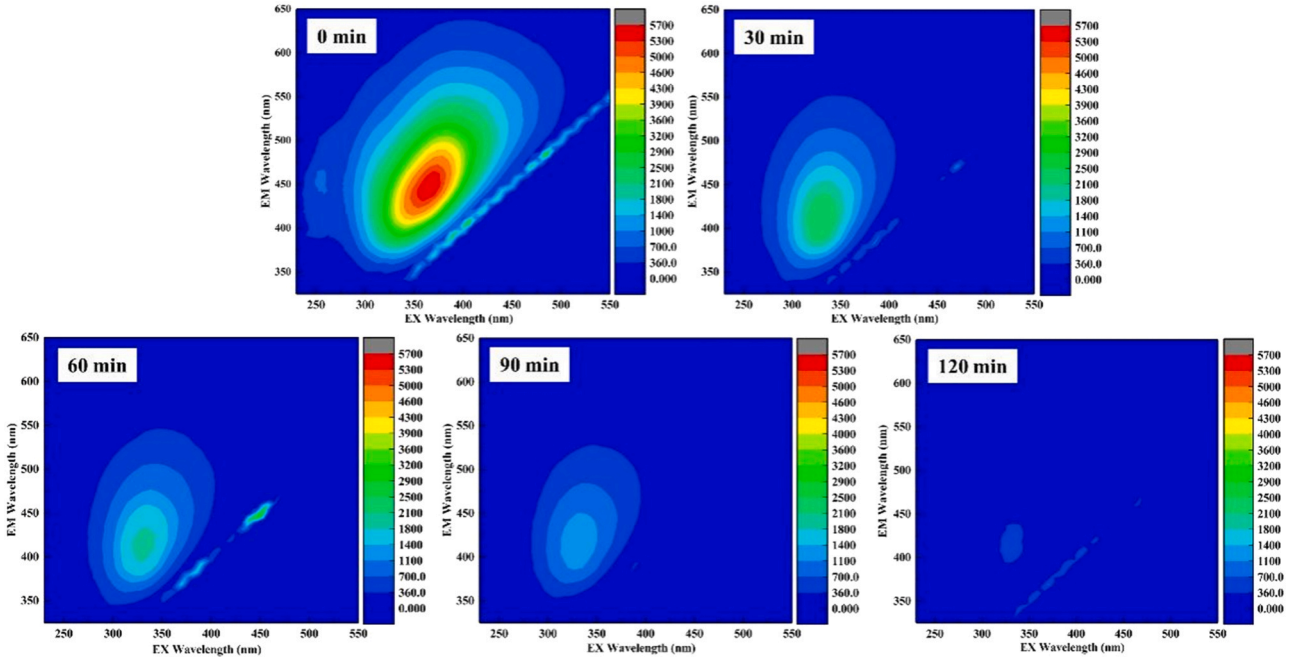

Fig. 8. Three-dimensional fluorescence spectra of polluted groundwater at different time points during treatment.

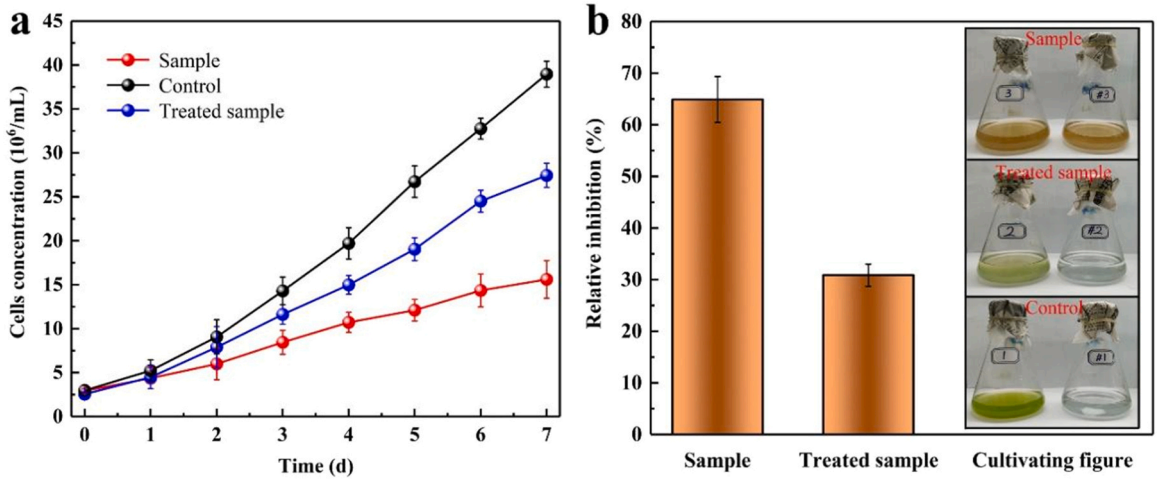

Fig. 9. The toxicity levels of untreated polluted groundwater, and the samples treated by NCP/PMS system: (a) changes of *Chlorella pyrenoidosa* cells concentration over time, and (b) calculated relative inhibition rates.

3.7. Toxicity alteration

The toxicity alteration of polluted groundwater before and after the reaction was manifested as the growth inhibition of the samples on *Chlorella pyrenoidosa*. It can be seen from Fig. 9a that the unprocessed sample significantly inhibit the growth of *Chlorella pyrenoidosa* ($P < 0.05$), and the cell concentration (15.61×10^6 cells/mL) of *Chlorella pyrenoidosa* is about 1/3 of that of the control group (38.96×10^6 cells/mL), indicating that groundwater polluted by aged landfill leachate have a high toxicity. Meanwhile, the cell concentration of *Chlorella pyrenoidosa* (27.44×10^6 cells/m) in the wastewater treated by NCP/PMS system is about doubled compared with that in the untreated wastewater, which indicate that the toxicity of wastewater treated by NCP/PMS system is significantly reduced. However, compared with the control group, there is still a certain degree of toxicity, which may be due to some toxic intermediate products produced by some organic substances in the wastewater after advanced oxidation treatment. Studies have shown that SR-AOPs has an excellent removal effect on refractory organic compounds (e.g. diclofenac phenol and sulfamethoxazole), but it will increase the toxicity of wastewater [70–72]. In addition, the relative inhibition rates of the polluted groundwater before and after treatment on *Chlorella pyrenoidosa* are 65% and 30%, respectively (Fig. 9b). The insets are the culture image of *Chlorella pyrenoidosa* in different samples on day 7 (blank control on the right). Therefore, NCP/PMS system not only has a good degradation effect on the organic compounds in polluted groundwater, but also reduces its biological toxicity.

3.8. Reusability of the NCP catalysts

The reusability of NCP in NCP/PMS system was evaluated by four-cycles experiments. After each experiment, NCP was collected by centrifugation and washed three times with deionized water and ethanol, respectively. Finally, NCP was dried in the oven, and ground for

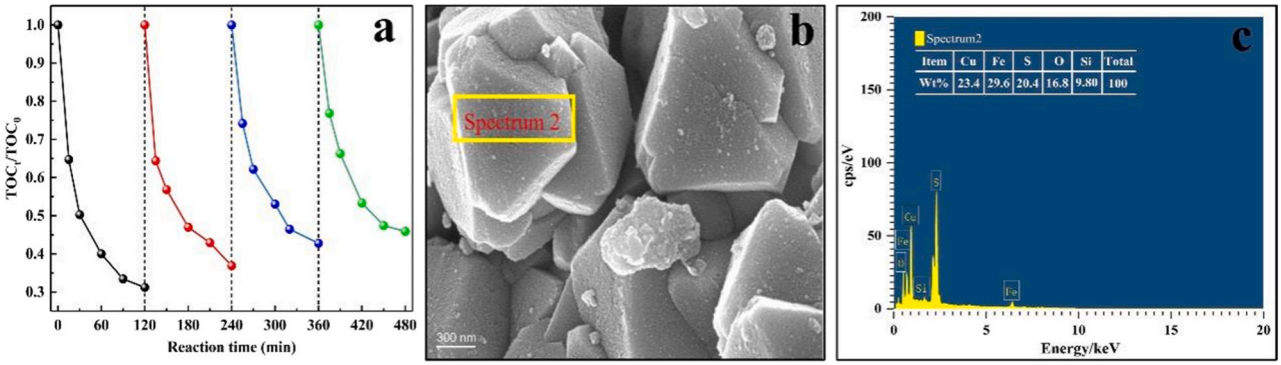

Fig. 10. (a) The reusability of NCP in NCP/PMS system. Experimental conditions: $[NCP]_0 = 10$ g/L, $[PMS]_0 = 25$ mM and initial pH $= 8.0 \pm 0.1$; (b) SEM image and (c) EDS of used NCP.

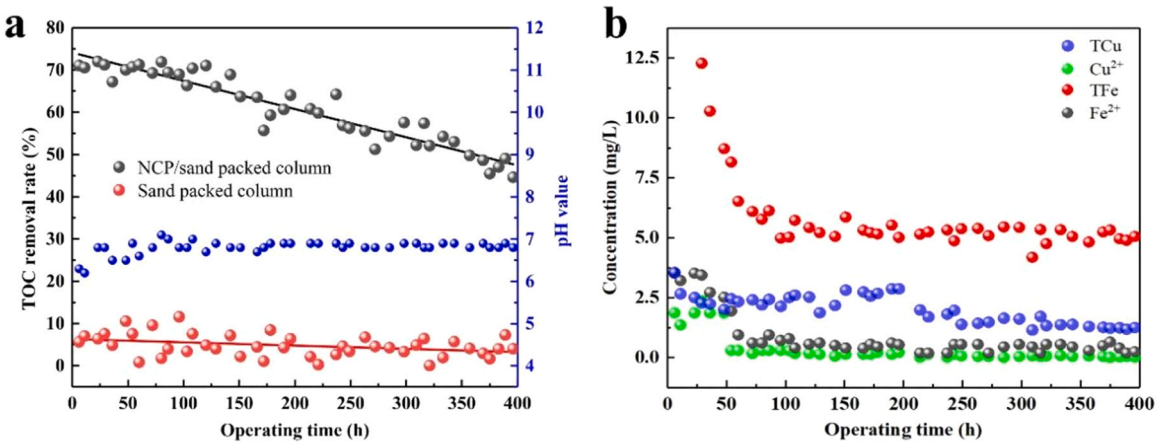

Fig. 11. The changes of (a) TOC degradation rate and effluent pH; (b) metal ion concentration.

the next cycle experiment. It can be seen from Fig. 10a, the ratio of TOC_t/TOC_0 decreases slightly after each recycle and its ratio decreases by nearly 20% after four-cycles. This may be related to the changes in the physicochemical properties of NCP before and after the reaction. In order to better reveal its changes, the used NCP was characterized. As shown in Fig. 1a, the positions of the substance peaks in used NCP remain unchanged and are nearly similar with fresh NCP. However, compared with fresh NCP, the peak intensity of used NCP decreases slightly after the reaction, which may be related to the dissolution of a small amount of metal ions in NCP and the change of crystal structure. By comparing the SEM images of fresh and used NCP (Figs. 1d and 4c), the overall structure of used NCP (Fig. 10b) shows no significant difference after the reaction, while the used NCP surface become rougher, because the NCP is corroded after the oxidation reaction. In addition, the EDS of used NCP is shown in Fig. 10c. Compared with EDS of fresh NCP, the peak strength of Cu Fe and S decrease significantly, and the ratio of Cu Fe and S on the surface of NCP decrease, while the ratio of O element increases, indicating that NCP is continuously oxidized and the products formed after oxidation cover the surface of NCP, leading to the decline of catalyst activity.

3.9. Performance of NCP/PMS in sand column

Fig. 11a shows the change of TOC removal rate of polluted groundwater after passing through sand column at different time points (NCP/sand—filling column and pure sand—filling column). As can be seen that the TOC removal rate of effluent water remains at about 70% in the first 5 days of operation of NCP/sand—filling column. With the extension of time, the TOC removal rate of contaminated groundwater shows a gradually decreasing trend. After 16 consecutive days, the TOC removal ability decreases by about 20%. The results show that the degradation ability of NCP to organic compounds in polluted groundwater is weakened under continuous water inflow, which may be due to the metal ion leaching and surface passivation on NCP with the increase of reaction time, resulting in the weakened activation ability of PMS, thus reducing the degradation efficiency of organic compounds. However, it is worth noting that after 16 days of reaction, the TOC removal rate remains above 45%, indicating a certain stability of NCP. At the same time, the results of the control group of pure quartz sand column showed that the TOC removal rate of polluted groundwater fluctuates between 0% and 10%, which may be because PMS itself has a certain ability to degradation of organic matter in polluted groundwater, which is consistent with the results in 3.2 section.

In addition, pH, as an important parameter of groundwater, is of great significance to the groundwater environment. Therefore, the pH of the NCP/sand—filling column effluent was monitored. It can be seen from the Fig. 11a that the pH fluctuates greatly in the first 5 days, which may be the operation of the system is not stable. As time goes by, the pH value is close to 7, and the effluent is neutral. This is inconsistent with the results in Section 3.4.2 (reaction for 120 min under optimal conditions, pH finally stabilizes at 4, and the solution is acidic). This may be due to the fact that the batch experiment was carried out in a beaker and the H^+ produced by the reaction would be continuous accumulation, and the column experiment is carried out in a continuous flow state, so there is a certain difference in pH, which further shows that NCP activation of PMS to repair organic polluted groundwater has a certain practicability. In order to understand the dissolution of metals under the condition of continuous flow of NCP, the concentrations of TFe, Fe^{2+}, TCu, and Cu^{2+} in the effluent water at different time points were monitored (Fig. 11b). During the first three days of operation, the

concentrations of TFe, Fe^{2+}, TCu and Cu^{2+} decrease gradually with the extension of time, in which the concentrations of TFe and Fe^{2+} change the most, indicating that the dissolution of metal iron is the main form of NCP during operation. After 3 days, the concentrations of TFe, Fe^{2+}, TCu and Cu^{2+} are respectively maintained at about 5.0, 0.5, 2.5 and 0.1 mg/L, which indicate that the filtered copper and iron were mainly Fe^{2+} and Cu^{+}.

4. Conclusions

In this study, NCP was used as a PMS activator for the remediation of groundwater by aged landfill leachate. Above all, the degradation efficiency of NCP/PMS system for organic matter in polluted groundwater is significantly better than that of NCP/PDS and NCP/H_2O_2, the removal rates of TOC and CN are 69% and 99%, respectively. Then, NCP dosage, PMS concentration and initial pH were explored through a single factor experiment, and the optimal remediation effect of polluted groundwater was achieved at pH 8, PMS concentration 25 mM and NCP dosage 10 g/L via response surface method (RSM) with Box–Behnken design (BBD) model. Meanwhile, the significance of the effect on TOC removal rate is as follows: NCP dosage>PMS concentration>initial pH value, and the removal rates of TOC and CN within 120 min were respectively 71% and 99% under the optimal experimental conditions. Furthermore, $SO_4^{\bullet-}$ and $^{\bullet}OH$ were the dominant active oxygen species in the NCP/PMS system with different initial pH, but the generation of $SO_4^{\bullet-}$ and $^{\bullet}OH$ were maximum at pH 8. Moreover, the complex organic compounds such as humus and aromatic compounds in the polluted groundwater were effectively degraded in the system, and the concentration and molecular weight of the organic compounds were greatly reduced. The growth inhibition rate of *Chlorella pyrenoidosa* was reduced by 35% after remediation, and the toxicity was significantly reduced. In addition, the activation performance of NCP decreased slightly after each recycle, but the degradation efficiency of TOC by NCP/PMS was still above 50%. Ultimately, in the flowing experiment using a vertical one-dimensional NCP/sand—filled column, the NCP/PMS system had excellent remediation performance for polluted groundwater in a flowing state at the initial stage of a long-term running and the filtered copper and iron were mainly Fe^{2+} and Cu^{+}. In brief, the study successfully confirmed the feasibility of NCP/PMS system for remediation of groundwater pollution in practice, and provided data and theoretical support for in-situ remediation of groundwater polluted by difficult degradable organic matter.

CRediT authorship contribution statement

Hongxi Wang: Data curation, Investigation, Drawing, Software, Original draft preparation. **Bing Liao:** Conceptualization, Funding acquisition, Supervision, Project administration, Writing – review & editing. **Mengyao Hu:** Writing – review & editing, Instrumental, Methodology. **Yulu Ai:** Writing – review & editing, Methodology, Data curation. **Lijia Wen:** Software, Methodology, Writing – review & editing. **Shuang Yang:** Methodology, Software. **Zhong Ye:** Writing – review & Editing. **Jie Qin:** Writing – review & editing. **Guo Liu:** Funding acquisition, Supervision, Validation, Writing – review & editing.

Declaration of Competing Interest

The authors declare that they have no known competing financial interests or personal relationships that could have appeared to influence the work reported in this paper.

Acknowledgments

We greatly acknowledged the financial support from the National Natural Science Foundation of China (No. 42007168), State Key Laboratory of Geohazard Prevention and Geoenvironment Protection Independent Research Project (SKLGP2019Z008) and the Cultivating Program of Young and Middle-Aged Key Teachers of Chengdu University of Technology (No. 10912-JXGG-06836).

Appendix A. Supporting information

Supplementary data associated with this article can be found in the online version at doi:10.1016/j.apcatb.2021.120744.

References

[1] W. Chen, A. Zhang, G. Jiang, Q. Li, Transformation and degradation mechanism of landfill leachates in a combined process of SAARB and ozonation, Waste Manag. 85 (2019) 283–294.
[2] D. Sun, X. Hong, Z. Cui, Y. Du, K.S. Hui, E. Zhu, K. Wu, K.N. Hui, Treatment of landfill leachate using magnetically attracted zero-valent iron powder electrode in an electric field, J. Hazard. Mater. 388 (2020), 121768.
[3] C. Amor, D.T. Estefanía, J.A. Peres, M.I. Maldonado, I. Oller, S. Malato, M.S. Lucas, Mature landfill leachate treatment by coagulation/flocculation combined with Fenton and solar photo-Fenton processes, J. Hazard. Mater. 286 (2015) 261–268.
[4] N.B. Azmi, M.J.K. Bashir, S. Sethupathi, L.J. Wei, N.C. Aun, Stabilized landfill leachate treatment by sugarcane bagasse derived activated carbon for removal of color, COD and NH3-N – optimization of preparation conditions by RSM, J. Environ. Chem. Eng. 3 (2015) 1287–1294.
[5] S.V. Niveditha, R. Gandhimathi, Flyash augmented Fe3O4 as a heterogeneous catalyst for degradation of stabilized landfill leachate in Fenton process, Chemosphere 242 (2020), 125189.
[6] D. Karimipourfard, R. Eslamloueyan, N. Mehranbod, Heterogeneous degradation of stabilized landfill leachate using persulfate activation by CuFe2O4 nanocatalyst: an experimental investigation, J. Environ. Chem. Eng. 8 (2020), 103426.
[7] X. Yang, L. Meng, F. Meng, Combination of self-organizing map and parallel factor analysis to characterize the evolution of fluorescent dissolved organic matter in a full-scale landfill leachate treatment plant, Sci. Total Environ. 654 (2019) 1187–1195.
[8] K.Y. Foo, L.K. Lee, B.H. Hameed, Batch adsorption of semi-aerobic landfill leachate by granular activated carbon prepared by microwave heating, Chem. Eng. J. 222 (2013) 259–264.
[9] Z. Han, H. Ma, G. Shi, L. He, L. Wei, Q. Shi, A review of groundwater contamination near municipal solid waste landfill sites in China, Sci. Total Environ. 569-570 (2016) 1255–1264.
[10] Z. Li, Q. Yang, Y. Zhong, X. Li, L. Zhou, X. Li, G. Zeng, Granular activated carbon supported iron as a heterogeneous persulfate catalyst for the pretreatment of mature landfill leachate, RSC Adv. 6 (2016) 987–994.
[11] W. Li, T. Hua, Q. Zhou, S. Zhang, F. Li, Treatment of stabilized landfill leachate by the combined process of coagulation/flocculation and powder activated carbon adsorption, Desalination 264 (2010) 56–62.
[12] S. Nazia, N. Sahu, V. Jegatheesan, S.K. Bhargava, S. Sridhar, Integration of ultrafiltration membrane process with chemical coagulation for proficient treatment of old industrial landfill leachate, Chem. Eng. J. 412 (2021), 128598.
[13] M.A.M. Reshadi, A. Bazargan, G. McKay, A review of the application of adsorbents for landfill leachate treatment: Focus on magnetic adsorption, Sci. Total Environ. 731 (2020), 138863.
[14] S. Cortez, P. Teixeira, R. Oliveira, M. Mota, Ozonation as polishing treatment of mature landfill leachate, J. Hazard Mater. 182 (2010) 730–734.
[15] Y. Deng, R. Zhao, Advanced Oxidation Processes (AOPs) in wastewater treatment, Curr. Pollut. Rep. 1 (2015) 167–176.
[16] F. Ghanbari, M. Moradi, Maternal hypothyroidism: an overview of current experimental models, Life Sci. 187 (2017) 1–8.
[17] M.G. Antoniou, A. Armah, D.D. Dionysiou, Degradation of microcystin-LR using sulfate radicals generated through photolysis, thermolysis and e− transfer mechanisms, Appl. Catal. B: Environ. 96 (2010) 290–298.
[18] A. Tsitonaki, B. Petri, M. Crimi, H. Mosbæk, R.L. Siegrist, P.L. Bjerg, In situ chemical oxidation of contaminated soil and groundwater using persulfate: a review, Crit. Rev. Environ. Sci. Technol. 40 (2010) 55–91.
[19] W. Wang, H. Wang, G. Li, P.K. Wong, T. An, Visible light activation of persulfate by magnetic hydrochar for bacterial inactivation: efficiency, recyclability and mechanisms, Water Res. 176 (2020), 115746.
[20] W. Wang, H. Wang, G. Li, T. An, H. Zhao, P.K. Wong, Catalyst-free activation of persulfate by visible light for water disinfection: efficiency and mechanisms, Water Res 157 (2019) 106–118.
[21] W. Nie, Q. Mao, Y. Ding, Y. Hu, H. Tang, Highly efficient catalysis of chalcopyrite with surface bonded ferrous species for activation of peroxymonosulfate toward degradation of bisphenol A: a mechanism study, J. Hazard. Mater. 364 (2019) 59–68.
[22] X. Yang, D. Yue, C. Guo, S. Wang, X. Qian, Y. Zhao, Effective removal of chlorinated organic pollutants by bimetallic iron-nickel sulfide activation of peroxydisulfate, Chin. Chem. Lett. 31 (6) (2021) 1535–1539.
[23] Q. Wang, B. Wang, Y. Ma, S. Xing, Enhanced superoxide radical production for ofloxacin removal via persulfate activation with Cu-Fe oxide, Chem. Eng. J. 354 (2018) 473–480.
[24] L. Xiao, M. You, F. Pan, M. Liu, P. Yang, D. Xia, Q. Li, Y. Wang, J. Fu, CuFe2O4@GO nanocomposite as an effective and recoverable catalyst of peroxymonosulfate

activation for degradation of aqueous dye pollutants, Chin. Chem. Lett. 30 (12) (2019) 2216–2220.
[25] J. Fan, L. Gu, D. Wu, Z. Liu, Synthesis and antimicrobial evaluation of novel 1,2,4-triazole thioether derivatives bearing a quinazoline moiety, Mol. Divers. 22 (2018) 657–667.
[26] J. Peng, H. Zhou, W. Liu, Z. Ao, H. Ji, Y. Liu, S. Su, G. Yao, B. Lai, Insights into heterogeneous catalytic activation of peroxymonosulfate by natural chalcopyrite: pH-dependent radical generation, degradation pathway and mechanism, Chem. Eng. J. 397 (2020), 125387.
[27] Y. Zhao, H. An, J. Feng, Y. Ren, J. Ma, Impact of crystal types of AgFeO2 nanoparticles on the peroxymonosulfate activation in the water, Environ. Sci. Technol. 53 (2019) 4500–4510.
[28] L. Lai, H. Zhou, B. Lai, Heterogeneous degradation of bisphenol A by peroxymonosulfate activated with vanadium-titanium magnetite: performance, transformation pathways and mechanism, Chem. Eng. J. 349 (2018) 633–645.
[29] Y. Zhou, Y. Zhang, X. Hu, Synergistic coupling Co3Fe7 alloy and CoFe2O4 spinel for highly efficient removal of 2,4-dichlorophenol by activating peroxymonosulfate, Chemosphere 242 (2020), 125244.
[30] L. Wang, Y. Kang, S.Y. Liang, D.Y. Chen, Q.Y. Zhang, L.X. Zeng, J.W. Luo, F. Jiang, Synergistic effect of co-exposure to cadmium (II) and 4-n-nonylphenol on growth inhibition and oxidative stress of Chlorella sorokiniana, Ecotoxicol. Environ. Saf. 154 (2018) 145–153.
[31] X. Yu, J. Sun, G. Li, Y. Huang, Y. Li, D. Xia, F. Jiang, Integration of •SO4–based AOP mediated by reusable iron particles and a sulfidogenic process to degrade and detoxify Orange II, Water Res. 174 (2020), 115622.
[32] I. Shitanda, K. Takada, Y. Sakai, T. Tatsuma, Compact amperometric algal biosensors for the evaluation of water toxicity, Anal. Chim. Acta 530 (2005) 191–197.
[33] C. Liang, C.F. Huang, N. Mohanty, R.M. Kurakalva, A rapid spectrophotometric determination of persulfate anion in ISCO, Chemosphere 73 (2008) 1540–1543.
[34] W. Chen, A. Zhang, G. Jiang, Q. Li, Transformation and degradation mechanism of landfill leachates in a combined process of SAARB and ozonation, Waste Manag. 85 (2019) 283–294.
[35] C. Tizaoui, L. Bouselmi, L. Mansouri, A. Ghrabi, Landfill leachate treatment with ozone and ozone/hydrogen peroxide systems, J. Hazard Mater. 140 (2007) 316–324.
[36] Y. Shi, J. Li, D. Wan, J. Huang, Y. Liu, Peroxymonosulfate-enhanced photocatalysis by carbonyl-modified g-C3N4 for effective degradation of the tetracycline hydrochloride, Sci. Total Environ. 749 (2020), 142313.
[37] H. Zhao, X. Huang, J. Wang, Y. Li, R. Liao, X. Wang, X. Qiu, Y. Xiong, W. Qin, G. Qiu, Comparison of bioleaching and dissolution process of p-type and n-type chalcopyrite, Miner. Eng. 109 (2017) 153–161.
[38] K.T. Chen, C.J. Chiang, D. Ray, Hydrothermal synthesis of chalcopyrite using an environmental friendly chelating agent, Mater. Lett. 95 (2013) 172–174.
[39] J.S. Salla, G.L. Dotto, D. Hotza, R. Landers, K.B. Martinello, E.L. Foletto, Enhanced catalytic performance of CuFeS2 chalcogenide prepared by microwave-assisted route for photo-Fenton oxidation of emerging pollutant in water, J. Environ. Chem. Eng. 8 (2020), 104077.
[40] P. Rupa Ranjani, P.M. Anjana, R.B. Rakhi, Solvothermal synthesis of $CuFeS_2$ nanoflakes as a promising electrode material for supercapacitors, J. Energy Storage 33 (2021), 102063.
[41] J.M. Monteagudo, A. Durán, R. González, A.J. Expósito, In situ chemical oxidation of carbamazepine solutions using persulfate simultaneously activated by heat energy, UV light, Fe2+ ions, and H_2O_2, Appl. Catal. B: Environ. 176–177 (2015) 120–129.
[42] Y. Hong, J. Peng, X. Zhao, Y. Yan, B. Lai, G. Ya, Efficient degradation of atrazine by CoMgAl layered double oxides catalyzed peroxymonosulfate: optimization, degradation pathways and mechanism, Chem. Eng. J. 370 (2019) 354–363.
[43] O.S. Furman, A.L. Teel, R.J. Watts, Mechanism of base activation of persulfate, Environ. Sci. Technol. 44 (16) (2010) 6423–6428.
[44] C. Luo, J. Ma, J. Jiang, Y. Liu, Y. Song, Y. Yang, Y. Guan, D. Wu, Simulation and comparative study on the oxidation kinetics of atrazine by UV/H_2O_2, UV/HSO_5^- and UV/$S_2O_8^{2-}$, Water Res. 80 (2015) 99–108.
[45] W.G. Kuo, Decolorizing dye wastewater with Fenton's reagent, Water Res. 26 (1992) 881–886.
[46] Y. Zhou, Y. Zhang, X. Hu, Synergistic coupling Co3Fe7 alloy and CoFe2O4 spinel for highly efficient removal of 2,4-dichlorophenol by activating peroxymonosulfate, Chemosphere 242 (2020), 125244.
[47] S. Ghafari, H.A. Aziz, M.H. Isa, A.A. Zinatizadeh, Application of response surface methodology (RSM) to optimize coagulation-flocculation treatment of leachate using poly-aluminum chloride (PAC) and alum, J. Hazard. Mater. 163 (2009) 650–656.
[48] Q.K. Beg, V. Sahai, R. Gupta, Statistical media optimization and alkaline protease production from Bacillus mojavensis in a bioreactor, Process Biochem. 39 (2003) 203–209.
[49] A. Jawad, J. Lang, Z. Liao, A. Khan, J. Ifthikar, Z. Lv, S. Long, Z. Chen, Z. Chen, Waterpipe tobacco smoking prevalence among young people in Great Britain, 2013–2016, Eur. J. Public Health 28 (2018) 548–552.
[50] L. Lai, H. Ji, H. Zhang, R. Liu, B. Lai, Activation of peroxydisulfate by V-Fe concentrate ore for enhanced degradation of carbamazepine: Surface —V(III) and —V(IV) as electron donors promoted the regeneration of —Fe(II), Appl. Catal. B: Environ. 282 (2021) 119559.
[51] H. Li, F. Deng, Y. Zheng, L. Hua, C. Qu, X. Luo, Visible-light-driven Z-scheme rGO/Bi2S3–BiOBr heterojunctions with tunable exposed BiOBr (102) facets for efficient synchronous photocatalytic degradation of 2-nitrophenol and Cr(VI) reduction, Environ. Sci.: Nano 6 (2019) 3670–3683.
[52] S.H. Joo, A.J. Feitz, D.L. Sedlak, T.D. Waite, Quantification of the oxidizing capacity of nanoparticulate zero-valent iron, Environ. Sci. Technol. 39 (2005) 1263–1268.
[53] W.D. Oh, Z. Dong, G. Ronn, T.T. Lim, Surface-active bismuth ferrite as superior peroxymonosulfate activator for aqueous sulfamethoxazole removal: performance, mechanism and quantification of sulfate radical, J. Hazard. Mater. 325 (2017) 71–81.
[54] R. Yin, W. Guo, H. Wang, J. Du, X. Zhou, Q. Wu, H. Zheng, J. Chang, N. Ren, Selective degradation of sulfonamide antibiotics by peroxymonosulfate alone: direct oxidation and nonradical mechanisms, Chem. Eng. J. 334 (2018) 2539–2546.
[55] C. Droguett, R. Salazar, E. Brillas, I. Sirés, C. Carlesi, J.F. Marco, A. Thiam, Treatment of antibiotic cephalexin by heterogeneous electrochemical Fenton-based processes using chalcopyrite as sustainable catalyst, Sci. Total Environ. 740 (2020), 140154.
[56] D. Xia, H. He, H. Liu, Y. Wang, Q. Zhang, Y. Li, A. Lu, C. He, P.K. Wong, Persulfate-mediated catalytic and photocatalytic bacterial inactivation by magnetic natural ilmenite, Appl. Catal. B: Environ. 238 (2018) 70–81.
[57] H. Chen, Z. Zhang, Z. Yang, Q. Yang, B. Li, Z. Bai, Heterogeneous fenton-like catalytic degradation of 2,4-dichlorophenoxyacetic acid in water with FeS, Chem. Eng. J. 273 (2015) 481–489.
[58] U. Rajaji, K. Murugan, S.M. Chen, M. Govindasamy, T.W. Chen, P.H. Lin, P. Lakshmi prabha, Graphene oxide encapsulated 3D porous chalcopyrite (CuFeS2) nanocomposite as an emerging electrocatalyst for agro-hazardous (methyl paraoxon) detection in vegetables, Compos. Part B: Eng. 160 (2019) 268–276.
[59] A. Ghahremaninezhad, D.G. Dixon, E. Asselin, Electrochemical and XPS analysis of chalcopyrite (CuFeS2) dissolution in sulfuric acid solution, Electrochim. Acta 87 (2013) 97–112.
[60] Y. Zhou, X. Wang, C. Zhu, D.D. Dionysiou, G. Zhao, G. Fang, D. Zhou, New insight into the mechanism of peroxymonosulfate activation by sulfur-containing minerals: role of sulfur conversion in sulfate radical generation, Water Res. 142 (2018) 208–216.
[61] X. Zhang, H. Deng, G. Zhang, F. Yang, G.-E. Yuan, Natural bornite as an efficient and cost-effective persulfate activator for degradation of tetracycline: Performance and mechanism, Chem. Eng. J. 381 (2020), 122717.
[62] D. Karimipourfard, R. Eslamloueyan, N. Mehranbod, Heterogeneous degradation of stabilized landfill leachate using persulfate activation by CuFe2O4 nanocatalyst: an experimental investigation, J. Environ. Chem. Eng. 8 (2020), 103426.
[63] L. Wang, F. Wu, R. Zhang, W. Li, H. Liao, Characterization of dissolved organic matter fractions from Lake Hongfeng, Southwestern China Plateau, J. Environ. Sci. 21 (2009) 581–588.
[64] R. Artinger, C. Buckau, S. Geyer, P. Fritz, M. Wolf, J.I. Kim, Characterization of groundwater humic substances: influence of sedimentary organic carbon, Appl. Geochem. 15 (2000) 97–116.
[65] S. Tao, J. Cui, C. Zhang, Acta Geogr. Sin. 45 (1990) 484–489.
[66] Q.Q. Zhang, B.H. Tian, X. Zhang, A. Ghulam, C.R. Fang, R. He, Investigation on characteristics of leachate and concentrated leachate in three landfill leachate treatment plants, Waste Manag. 33 (2013) 2277–2286.
[67] W. Chen, P. Westerhoff, J.A. Leenheer, K. Booksh, Fluorescence excitation-emission matrix regional integration to quantify spectra for dissolved organic matter, Environ. Sci. Technol. 37 (2003) 5701–5710.
[68] A. Baker, M. Curry, Fluorescence of leachates from three contrasting landfills, Water Res. 38 (2004) 2605–2613.
[69] W. Chen, Y. Luo, G. Ran, Q. Li, An investigation of refractory organics in membrane bioreactor effluent following the treatment of landfill leachate by the O3/H2O2 and MW/PS processes, Waste Manag. 97 (2019) 1–9.
[70] X. Lu, Y. Shao, N. Gao, J. Chen, Y. Zhang, H. Xiang, Y. Guo, Degradation of diclofenac by UV-activated persulfate process: Kinetic studies, degradation pathways and toxicity assessments, Ecotoxicol. Environ. Saf. 141 (2017) 139–147.
[71] D. Xia, R. Yin, J. Sun, T. An, G. Li, W. Wang, H. Zhao, P.K. Wong, Natural magnetic pyrrhotite as a high-efficient persulfate activator for micropollutants degradation: radicals identification and toxicity evaluation, J. Hazard. Mater. 340 (2017) 435–444.
[72] C. Qi, X. Liu, C. Lin, X. Zhang, J. Ma, H. Tan, W. Ye, Degradation of sulfamethoxazole by microwave-activated persulfate: Kinetics, mechanism and acute toxicity, Chem. Eng. J. 249 (2014) 6–14.